Fog Presence and Ecosystem Responses in a Managed Coast Redwood Forest

A Thesis

SUBMITTED TO THE FACULTY OF THE UNIVERSITY OF MINNESOTA BY

Julia Petreshen

IN PARTIAL FULFILLMENT OF THE REQUIREMENTS FOR THE DEGREE OF

MASTER OF EARTH SCIENCES

Dr. Salli Dymond

May 2021

Acknowledgements

I gratefully acknowledge support from the National Science Foundation (NSF-EAR-1807165), the Pacific Southwest Research Station of the U.S. Forest Service, and the California Department of Forestry and Fire Protection for funding this research. I'd like to thank the Department of Earth and Environmental Sciences for their support through fellowships and assistantships over the past two years.

My greatest thanks are extended to the incredible mentors I've had the pleasure of working with. First, I'd like to thank my advisor, Dr. Salli Dymond, who has provided an immense amount of support and encouragement. Salli, thank you for giving me a little push when I needed to grow, supporting all my wildest ideas, and keeping it together when it seemed like the world was unraveling. I would also like to thank my committee members, Dr. Joseph Wagenbrenner and Dr. Byron Steinman, whose ideas and support were essential to the study design and statistical analysis.

I would like to thank my Caspar Creek field family – Liz Keppeler and every member of the field crew. Thank you for inspiring the project, assisting with programming, and tending to the study sites while I was away. A special thanks to Brian Storms for support and patience in climbing trees, setting tricky lines, and retrieving them when I got them stuck. Thank you to the additional field crew members that assisted with sensor deployment: Kevin Mazzocco, Megan Arnold, Ellen Sue Rickels, John Whiting, and Serena Kuczmarski. Big thanks to Tyler Burke for providing food, housing, help with construction, and hunting down materials for the project.

Finally, I would like to thank all my friends, family, and fellow graduate students for both technical and emotional support. I am especially grateful for Erika Winner, who

provided nourishment, encouragement, and many laughs during long field days and long writing days. Thank you to Eleanor Ludkey, Serena Kuczmarski, Derek DiOrio, Shelby Hammerschmidt, and Emma Burgeson for being there when I needed it most. Lastly, thank you to my incredible family for supporting me while I chase my wildest dreams.

Dedication

Для Мами і Тата, хто мені відкрили ці всі можливості – я дякую вам.

For Mom and Dad, who opened the door to all these opportunities – I thank you.

ABSTRACT

Fog inundation along California's Coast Range creates microclimates that support coast redwood (*Sequoia sempervirens*, D. Don) forests during the summer drought period. With changes in land use and climate, the coast redwood ecosystem is susceptible to increased drought stress. Thus, understanding the role of fog in relieving drought stress is important to properly manage the remaining coast redwood forests. Fog presence and ecosystem responses (e.g., climate, soil moisture, sap flow) were monitored at the Caspar Creek Experimental Watersheds in northwestern California over the 2020 fog season (Jun – Sept). Observations were recorded at shoulder and ridge topographic positions in harvested and unharvested third-growth forest to examine 1) temporal and spatial distribution of fog, 2) soil moisture responses to fog events, and 3) the influence of fog on transpiration. Fog presence was found to vary across the landscape with no significant relationship to harvesting. Fog deposition was higher at the shoulder position than at the ridge of the hillslope. Small increases in soil and litter moisture were observed at all study sites in response to fog events, with high temporal variation through the season. Surficial soil moisture was highest near the boles of *S. sempervirens* trees at the shoulder hillslope positions, regardless of harvest condition. All sites displayed lower transpiration rates during fog periods, but the greatest reduction was at the harvested sites. Overall, this research suggests that the distribution of fog and its ecological effects at the Caspar Creek Experimental Watersheds is primarily driven by topography and species composition rather than forest density.

TABLE OF CONTENTS

LIST OF TABLES

LIST OF FIGURES

LIST OF ABBREVIATIONS

Abbreviation	Definition
AMS	American Meteorological Society
ANOVA	Analysis of Variance
CAL FIRE	California Department of Forestry and Fire Protection
CCEW	Caspar Creek Experimental Watersheds
CI	Confidence Interval
CSI	Campbell Scientific, Inc.
DBH	Diameter at Breast Height
df	Degrees of Freedom
FLCC	Fog and Low Cloud Cover
GWC	Gravimetric Water Content
HRM	Heat Ratio Method
HSD	Honestly Significant Difference
LAI	Leaf Area Index
LWS	Leaf Wetness Sensor
MABL	Marine Atmospheric Boundary Layer
MET1	Meteorological Station
MSC	Maximum Significance Coefficient
PAR	Photosynthetically Active Radiation
PPT	Precipitation
RH	Relative Humidity
SD	Standard Deviation
SFM1	Sap Flow Meter
VPD	Vapor Pressure Deficit
VWC	Volumetric Water Content

1. INTRODUCTION

Fog inundation along coastal mountain regions creates microclimates that result in unique ecological communities. One of the most considerable microclimate influences of fog on ecosystems is in relieving plant water stress - sometimes to the extent of setting apart ecological communities across small geographic areas. Coastal mountain regions generate fog through orographic and/or advective forces that cool an air mass to its dew point and transport it across the landscape. Along the eastern Pacific Ocean, the upwelling of the California Current drives fog formation along the coast of California and relieves seasonal droughts that are characteristic of its typical Mediterranean climate. Vegetation within Mediterranean climates rely on winter rains as the primary input to the annual water budget, as the summer season receives little-to-no precipitation. Along the California coastline, however, the frequent fog and stratus clouds that are common in otherwise dry summer months have created a microclimate that supports coast redwood forests. Dominated by the tallest living tree species (*Sequoia sempervirens*, D. Don), the narrow distribution of the coast redwood forest is limited to the fog inundated zone along the California coast, locally referred to as the "fog belt."

Fog presence relieves water stress in the coast redwood forest by reducing the amount of water lost through evapotranspiration and directly supplying water to plants. Lower temperatures and increased humidity associated with fog presence reduce the vapor pressure deficit that drives evapotranspiration. Sap flow is typically used to measure the rate of transpiration and consequently, plant growth and the amount of water lost to the atmosphere. During fog events, sap flow in *S. sempervirens* is often reduced and, in some cases, reversed (Burgess and Dawson, 2004; Simonin et al., 2009). Sap flow reversal

indicates fog water is being directly absorbed through foliage, which has been observed in 80% of the dominant overstory and understory species of the coast redwood forest (Limm et al., 2009). This absorbed fog water may then be used to refill desiccated plant tissues and maintain growth during periods of low rainfall.

Accumulated fog water on foliage can also grow to large droplets and generate "fog drip" or "fog precipitation". Fog drip contributes to water stored in the soil, where it is further available for plants via root uptake. Plant transpiration is typically dependent on the availability of soil water, and low soil moistures have been found to reduce growth of *S. sempervirens* (Olson et al., 1990). The deposition of water as fog precipitation has been a long-studied phenomenon along the California coast due to its role in relieving seasonal drought (Means, 1927; Oberlander, 1956; Azevedo and Morgan, 1974; Dawson, 1998) and increasing soil moisture (Ewing et al., 2009; Carbone et al., 2011). When fog deposition is observed, it often improves plant water status by increasing soil moistures (Dawson, 1998; Ewing et al., 2009; Fischer et al., 2016). However, the magnitude and extent of deposition along a soil profile varies across studies and is influenced by a range of site characteristics (Ingraham and Matthews, 1995; Dawson, 1998; Ewing et al., 2009; Carbone et al., 2013; Fischer et al., 2016; Cárdenas et al., 2017).

Fog interception and its volumetric input to an ecosystem depend on local topography, climate, and forest structure. Along the California coast, fog interception occurs when it is transported from the Pacific Ocean across the landscape by wind. High temperatures and wind speeds may cause fog to dissipate before deposition occurs. Fog deposition generally increases with elevation; vegetation at higher topographic positions is fully enveloped in the fog and low cloud layers and maintains prolonged contact with

suspended fog water particles. Changes in land use by natural or anthropogenic forces may alter forest structure and change the way fog interacts with ecosystems. Timber harvest within the coast redwood forest is a common land use practice, and results in changes to the forest structure from reduced stand densities. Stand density and fog interception are a commonly studied relationship along the Pacific coast (Harr, 1982; Ingwersen, 1985; Dawson, 1998) and around the world (Ataroff and Rada, 2000; Barbosa et al., 2010). However, the relationship between fog interception and stand density are unclear in literature. Some studies indicate that the greatest fog interception and deposition occur at forest edges based on their direct exposure to winds (Ewing et al., 2009). Other studies show that fog deposition is greatest in closed canopy systems, where canopy surfaces increase interception and reduce the evaporation of deposited fog water (Dawson, 1998; Barbosa et al., 2010).

Along the California coast, warming sea-surface temperatures are driving a decline in fog and stratus cloud occurrence (Johnstone and Dawson, 2010). This decline has profound implications for maintaining the health and distribution of the coast redwood forest. With a decline in fog presence, the narrow distribution of the coast redwood forest may be further reduced due to stress experienced by drought conditions. Changes in forest structure have caused varying responses in fog deposition. Since fog is transported horizontally across the landscape by wind, it is difficult to measure using standard rain gauges. The challenges associated with measuring fog presence leads to difficulty in quantifying its hydrologic contribution to an ecosystem. Previous studies reveal the unpredictable nature of fog distribution and resulting ecosystem responses in coastal ecosystems (Azevedo and Morgan, 1974; Fischer and Still, 2007; Fischer et al., 2016),

including coast redwood forests (Dawson, 1998; Burgess and Dawson, 2004; Ewing et al., 2009). However, more research is needed to characterize fog deposition and identify its role in relieving the effects of seasonal drought in varying forest structures. This study expands upon our current understanding of fog distribution and examines the influence of timber harvest on fog deposition in a managed third-growth coast redwood forest.

2. STUDY QUESTIONS

The overarching goal of this study was to assess fog presence and compare the influence of timber harvest on the ecosystem functions of fog in the coast redwood forest. More specifically, my research addressed the following questions:

Question 1: How does canopy cover influence the intensity and duration of leaf wetness caused by fog?

Hypothesis: There will be no significant difference in the intensity or duration of leaf wetness caused by fog between the harvested and forested sites.

Explanation: Openings associated with reduced canopies allow incoming solar radiation and wind turbulence to drive evaporation and dissipate fog (Dawson, 1998). Wind speeds decrease as they meet frictional surfaces such as forest canopies, so harvested sites are expected to experience higher wind speeds than forested sites. Therefore, as fog rolls onto the landscape, it is expected to remain at the forested sites at its full intensity, reflected by higher intensities of leaf wetness. At the harvested sites, however, evaporation and high wind speeds will cause fog to dissipate, leading to lower leaf wetness and/or shorter fog events.

Question 2: How does litter and soil moisture following fog events compare between forested and harvested sites?

Hypothesis: Harvested and forested sites will have no significant difference in surficial soil and litter water content following fog events.

Explanation: Rates of fog deposition are related to stand density, with greater densities containing more fog-intercepting surfaces and typically generating higher volumes of fog deposition (Dawson, 1998; Barbosa et al., 2010). In canopy openings, fog water delivered to forest litter can be evaporated, thereby never becoming part of the stored soil or litter moisture. Greater canopy cover creates shading from incoming solar radiation and reduces the rate of evaporation. Therefore, due to more fog-intercepting surfaces and lower evaporation rates, the forested sites are expected to have higher surficial soil and litter moisture levels than the harvested sites.

Question 3: How do the changes in transpiration following fog presence compare between forested and harvested sites?

Hypothesis: The presence of fog will cause a similar reduction in transpiration at the harvested and forested sites.

Explanation: As mentioned above, canopy openings allow more incoming solar radiation and higher wind speeds, leading to higher temperatures and vapor pressure deficit (VPD) which drive evapotranspiration. The VPD is typically reduced or eliminated during fog presence, causing a reduction in evapotranspiration (Burgess and Dawson, 2004; Limm et al., 2009; Earles et al., 2015). Harvested sites are expected to have greater VPD and evapotranspiration rates than the forested sites. Therefore, when fog is present and

evapotranspiration is reduced, the greatest reduction is expected to occur at the harvested sites than the forested sites.

3. BACKGROUND

3.1 Fog Formation

Fog is defined as suspended water droplets near the ground surface that reduce visibility by one kilometer (AMS, 2012). Generally, fog is categorized as a type of low cloud whose base touches the ground. Fog is formed and influenced by many factors, making it difficult to classify. However, all fog types originate when water or land surface temperatures equal or near the dew point of the surrounding air mass (AMS, 2012).

Advection fog dominates along the California coast. The northern-hemisphere Hadley atmospheric circulation cell is responsible for the high pressure over the eastern North Pacific Ocean (Torregrosa et al., 2016). Commonly referred to as the Pacific High, it drives warm, dry air from the equator to descend over the region. The cool ocean surface and an overhead layer of warmer air traps the subsiding air mass. A strong temperature inversion creates the cool and humid marine atmospheric boundary layer (MABL) (Torregrosa et al., 2015; Rastogi et al., 2016). Fog is formed when a warm air mass becomes trapped within the MABL and cooled by the ocean surface. Periodically, the upwelling of cold ocean currents contributes to cooling the trapped air mass and forming fog along the coast of California. As land heats up over the course of the day, a low-pressure region develops and contrasts the Pacific High over the ocean. This pressure

difference is responsible for the north-northwesterly winds that develop along the coast and drive fog onto land (Rastogi et al., 2016). Fog events in coastal California follow a diurnal pattern; fog forms in the evenings, is the most present at night, and dissipates in the morning (Fischer and Still, 2007). Looking at the annual distribution of fog along coastal California, the fog season falls between the months of May and September, with July and August being the foggiest months (defining cloud-base heights at 21.1m as fog events) (Rastogi et al., 2016).

3.2 Interception of Fog

Fog is composed of small (4 – 10 μm) water droplets which, due to their small size, stay suspended in the air and rely primarily on wind for transport. As fog travels horizontally through a forest, it becomes intercepted by foliage, which provide surfaces for the small water droplets to accumulate on, which may then fall to the ground as larger water droplets. The permeability of a forest canopy allows moist air to pass through, while large foliage surface areas are efficient in capturing and storing fog water particles (Kerfoot, 1968).

Intercepted fog water has three fates depending on the fog event intensity and duration. During an intense or long-lasting fog event, small water particles saturate foliage and may accumulate on leaves and needles. Continued accumulation of water may exceed the storage capacity of this foliage, releasing them to fall or flow to the ground. If the storage capacity is not exceeded, fog water may evaporate back into the atmosphere at a rate determined by the vapor pressure deficit. Lastly, intercepted fog water can be absorbed by plant bark and foliage via a process called direct uptake (Dawson, 1998; Burgess and Dawson, 2004; Limm et al., 2009; Earles et al., 2015).

Accumulated fog water that falls directly out of the canopy is generally referred to as “fog precipitation” or “fog drip.” Fog precipitated out of the trees has been a long-studied phenomenon along the California coast (Means, 1927; Oberlander, 1956; Azevedo and Morgan, 1974; Dawson, 1998). Volumes of fog drip are related to the area and density of trees as well as their exposure to wind-blown fog (Harr, 1982). Water inputs by fog drip can significantly raise soil moisture levels and provide a source of water to shallow-rooted species during times of drought (Dawson, 1998; Fischer et al., 2009; Carbone et al., 2013). However, studies have displayed variation in fog drip inputs based on forest type, structure, and site-specific characteristics.

3.3 Fog Interception and Meteorological Conditions

Several meteorological factors affect the amount of fog intercepted by forest surfaces. Since wind is the primary driver of advective fog across the landscape, higher wind speeds suggest more contact between the fog-rich air and condensation surfaces, such as the foliage of forest vegetation. Total fog deposition is often a function of wind speed, with higher rates of deposition generally occurring at higher wind speeds (Pryet et al., 2012; Hiatt et al., 2012). A study conducted on Santa Cruz Island off the coast of southern California found almost all fog deposition occurring at wind speeds between 2-3 m/s (Fischer and Still, 2007). Along the northern California coast, the speed of northernly winds was the determining factor in fog frequency (Johnstone and Dawson, 2010). Since fog formation along the coast of California stems from the interaction with the Pacific Ocean, the direction of prevailing winds can indicate whether the transported air is carrying fog that formed over the ocean.

3.4 Fog Interception and Topography

Microclimates that result from local topography variability can cause variation in fog water deposition over relatively short distances. Since fog moves primarily horizontally across a landscape and very close to the ground surface, it is influenced by topographic and structural variations in the landscape. Fog studies conducted on coastal-inland transects found that volumes of collected fog water decrease with increased distance from the coast (Cáceres et al., 2007; Fischer and Still, 2007). The use of fog water by perennial grasses in coastal California likewise decreases as the distance from the coast increases (Corbin et al., 2005).

Orographic uplift, as well as proximity to the coast, can be responsible for variation in fog deposition. Fog drip is generally found to increase with elevation and decrease in frequency as distance from the coast increases (Fischer and Still, 2007; Holder, 2003). A study conducted in a Guatemalan rainforest found that fog deposition at a higher elevation site (2550 m) was more than eight times greater than at the lower elevation site (2100 m) (Holder, 2003). Water inputs and ecosystem water stress studied along a transect on an island off the coast of southern California examined the effect of both distance from the coast and elevation on water storage and drought stress. This study revealed sites closer to the coast benefitted from persistent cloud cover, which decreased with distance from the coast, while higher elevations generated greater fog drip (Figure 1) (Fischer et al, 2009). The height of the cloud layer drives the relationship between elevation and fog deposition. Higher rates of fog deposition with increased elevation is limited to the elevation of the cloud top (Figure 1). Once land elevation rises above the top of the cloud layer, vegetation is no longer enveloped in the cloud/fog. The

relationship between cloud bases and tops relative to land elevation can indicate whether a site is inundated in a cloud layer and capable of generating fog drip. Higher elevations are also correlated with higher wind speeds, which increase fog deposition as discussed above (Fischer and Still, 2007).

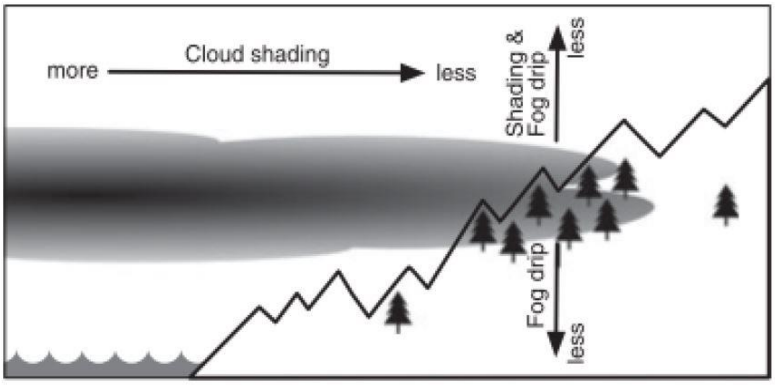

Figure 1: Conceptual model of cloud shading and fog drip distribution along a transect accounting for distance from coast and elevation. Arrows indicate cloud shading decreases with distance from the coast and fog drip decreases when outside the elevation band of the cloud layer. When land elevation is within the bands of the cloud base and cloud top, the landscape is experiencing fog and can generate fog drip. Figure by Fischer et al., 2009.

3.5 Fog Interception and Stand Density

The density of trees in a forest stand is a key component in intercepting and delivering fog water to the rest of the forest ecosystem. Natural or anthropogenic disturbances that reduce stand densities can alter fog interception rates. Tree basal area can be used as an index of crown size and, therefore, the vegetative surface area capable of intercepting wind-blown fog (Barbosa et al., 2010). Openings in the canopy associated with lower stand densities dissipate fog due to increased evaporation based on higher radiation and wind speeds (Dawson, 1998). In a fog-inundated coastal forest in Chile,

canopy patch area (related to total tree basal area) had a positive relationship with stemflow volumes, and soil and litter water contents (Barbosa et al., 2010). Similar findings have been revealed in coastal forests in California, which receive seasonal inputs of fog (Harr, 1982; Dawson, 1998). In a coast redwood forest, the average annual fog drip input was 34% in a forested stand, compared with 17% in a deforested stand (Dawson, 1998). Reduced fog drip related to timber harvest is significant enough to impact summer streamflow in other regions of the Pacific Northwest (Harr, 1982; Ingwersen, 1985). However, other studies indicate greater fog drip occurs along forest edges, which are maximized with selection-type timber harvest. Soil moisture resulting from fog deposition in a coast redwood forest was found to be greatest at the forest edge and decreasing with distance from the edge (Ewing et al, 2009).

Stand density influences not only the volumes of fog drip, but also the overall water storage ability of the forest. Smaller patches of forest have greater temperature fluctuations throughout the day than larger patches. The smaller temperature fluctuations in larger patches create a relatively stable microclimate compared to smaller ones (Barbosa et al., 2010). Removal of trees may alter the microclimates associated with the stands and change the ecosystem from a cool, moist environment to one that is more prone to the effects of droughts (Dawson, 1998). Canopy openings also allow more incoming solar radiation than closed-canopy systems. Increased solar radiation leads to increased vapor pressure deficit due to higher temperatures, causing more water loss by evapotranspiration with the removal of trees.

3.6 Fog as a Water Source to Plants

In coastal California, forest plants frequently use fog water to varying extents to relieve water stress (Ingraham and Matthews, 1995; Dawson, 1998; Corbin, 2005; Ewing et al., 2009; Hiatt et al., 2012; Fischer et al., 2016). One study in the coast redwood forest found *S. sempervirens* contained an average of ~18.6% fog water and understory plants contained ~66% fog water during the summer season (Dawson, 1998). Small trees and understory plants are more likely to rely on fog as a source of water because of their shallow roots that readily access water deposited by fog drip. Saplings are especially vulnerable during drought and benefit more from fog drip than adult trees due to their shallow roots (Baguskas et al., 2016).

Fog water becomes available for root uptake via fog drip, but some plants can use fog water directly from the atmosphere by a process termed "direct foliar uptake." In the redwood forest, over 80% of all dominant species exhibit the ability to directly uptake fog water through their leaves (Limm et al., 2009). *S. sempervirens* leaves were also found to directly absorb fog water, but the amount of water absorbed is small compared to what is lost during transpiration (Burgess and Dawson, 2004). Fog presence often reduces the vapor pressure deficit (VPD) and thus, transpiration, which is observed as a reduction in xylem sap flow rates. During intense fog events, sap flow was observed to reverse in *S. sempervirens* (Burgess and Dawson, 2004). This sap flow reversal indicates not only that transpiration losses cease, but also that atmospheric water absorbed by the leaves may be transported to the roots. The combination of direct foliar uptake and reduced transpiration provides relief from water stress for *S. sempervirens*. Since this phenomenon occurs primarily during the growing season, it may be responsible for the

fast growth and size of *S. sempervirens* (Burgess and Dawson, 2004). Bishop pine (*Pinus muricata*, D.Don) and Torrey pine (*Pinus torreyana* ssp. *Insularis* Haller), both endemic to the California fog belt like *S. sempervirens*, also experience higher basal growth when exposed to fog and cloud cover (Carbone et al., 2013; Williams et al., 2008). Fog thus is an important source of water to during the summer dry season.

3.7 Fog and Reduction of Evapotranspiration

Fog also relieves summer water stress by reducing evaporation and transpiration rates. The presence of fog has similar effects as cloud cover in that the provided shade reduces incoming solar radiation, which lowers air and leaf temperatures. Relative humidity during periods of fog inundation is reported to be close to or equal 100% (Tolle et al., 2005; Cáceres et al., 2007; Fischer et al., 2009). High humidity rates work to reduce the vapor pressure deficit (VPD) that drives evapotranspiration. VPD is calculated as the difference, or deficit, between the amount of water vapor in the air (i.e., actual vapor pressure) and the maximum amount of water vapor the air can hold (i.e., saturation vapor pressure) at a given temperature.

Low stratus clouds and fog events are frequently linked to reductions in evapotranspiration rates in various ecosystems (Hildebrandt et al., 2007; Ritter et al., 2008; Fischer et al., 2009; Saksa et al., 2014). In fact, the primary role of fog in relieving plant water stress is likely through reduction in evaporation and transpiration. Cloud cover and fog in a coastal pine ecosystem on Santa Cruz Island had lower rates of soil surface evaporation and largely relieved plant and microbial water stress (Carbone et al., 2013). In the study, sites that received lower total water inputs maintained higher levels of soil moisture over the summer season because they spent more time under fog and

cloud cover. Likewise, direct uptake of fog water by *S. sempervirens* can be relatively small, but the reduced transpiration and rehydration of leaves caused by fog deposition can be significant in reducing water stress (Burgess and Dawson, 2004).

Land use changes in fog-dependent ecosystems can significantly alter evaporation rates. Shading benefits provided by fog and cloud cover can also be achieved through canopy cover, therefore it is not surprising that ecosystems with reduced or eliminated canopy cover experience higher rates of evaporation from the soil surface (Ataroff and Rada, 2000; Fischer et al., 2016). On the other hand, undisturbed forest stands may experience more water loss from transpiration than soil evaporation alone at a harvested site (Ingwersen, 1985). Overall, fog presence is capable of significantly reducing evapotranspiration rates and ameliorating seasonal water stress.

3.8 Fog Water Inputs to Soil

Fog drip in forested ecosystems has long been observed and is known to increase soil moisture in areas where fog is "stripped" from the air (Oberlander, 1956; Parsons, 1960; Vogelmann et al., 1968; Azevedo and Morgan, 1974; Harr, 1982; Ingwersen, 1985; Schemenauer et al., 1988). Fog drip frequently contributes moisture to soils during the summer dry season. As fog drip infiltrates to the rooting zone, water becomes available for plant uptake (Ingraham and Matthews, 1995; Dawson, 1998; Fischer et al., 2016). This water input to the soil is critical in maintaining plant growth and survival since plants rely on soil moisture as their primary source of water. Periods of low soil moisture conditions have been linked to reduced rates of basal area growth of *S. sempervirens* (Olson et al., 1990). Water inputs to the soil by fog drip may also enter the hydrologic

cycle by contributing to summer streamflow (Harr, 1982) and recharging groundwater (Ingraham and Matthews, 1988; Ingraham and Matthews, 1995).

Since fog drip depends on the presence of intercepting surfaces, soil moisture responses to fog events vary with canopy cover. Over the course of a fog season, soils under canopy cover maintain a higher water content than soils outside the canopy (Ataroff and Rada, 2000; Fischer et al., 2009). Responses in soil moisture are often based on individual fog events that generate fog drip. Increases in soil moisture following these events are generally measured in the litter layer and upper portions of the soil profile. The depth at which pulses of moisture are measured in a soil profile varies among studies. Some studies report responses to fog drip are limited to the litter layer (Carbone et al., 2013). Other studies found fog drip within the upper 4 cm (Carbone et al., 2011), the upper 10 cm (Ewing et al., 2009), and as deep at 35 cm below the surface (Ewing et al., 2009). Examining the influence of fog drip on soil moisture inside and outside a canopy, Fischer et al. (2009) found fog drip to maintain soil moisture within the canopy three months after the last rainfall event. Soils outside the canopy dried below the permanent wilting point two weeks after the last rain.

3.9 Coast Redwood (*S. sempervirens*)

Coast redwoods (*S. sempervirens*) are the tallest living trees in the world and are endemic to the coastal areas of northern California and southwest Oregon. The natural distribution of *S. sempervirens* is a narrow belt ~450 miles long from 42º 09’ N. latitude (southwestern Oregon) to 35º 41’ N. latitude (southern Monterey County, California) (Noss et al., 2000). This distribution belt is between 5-35 miles wide with developed forests in the north and patchy stands in the southern extent of the range. The climate in

this region is Mediterranean, with wet, mild winters followed by rain-free summers. Because the summer season receives little water inputs from precipitation, frequent fog occurrence may be a factor in delineating the distribution of the *S. sempervirens* species (Olson et al., 1990; Noss, 2000).

S. sempervirens are thought to be efficient in intercepting fog from the atmosphere due to their high leaf area index (LAI) (Westman and Whittaker, 1975). Being able to capture fog aids the species during times of water stress, especially because *S. sempervirens* transpire significant amounts of water as the atmosphere dries. This water loss is caused by poor stomatal response to changes in the vapor pressure deficit or incompletely closing their stomates (Noss, 2000). *S. sempervirens* are a shade tolerant species due to their high photosynthetic capacity in low light environments. Soils in coast redwood forests are commonly moist and deep, usually in the Inceptisol or Ultisol soil orders (Olson et al., 1990). The root system of *S. sempervirens* is composed of lateral (fibrous) roots that grow deep and widespread, with no single taproot. Their roots rarely access groundwater sources and primarily rely on using shallow soil water (Burgess and Dawson, 2004). *S. sempervirens* seedlings are very sensitive to dry soils because they have no root hairs, making them inefficient at extracting water from the soil. Once established, seedlings can grow quickly; frequently up to 45 cm in the first season (Griffith, 1992). Adult trees exhibit annual radial growth beginning mid-March, peak in late May, and slowly decline until late September (Olson et al., 1990). *S. sempervirens* can sprout from the root crown, stem, or stump, making them resilient against natural disturbance regimes that can severely impact other species in the forest.

3.10 Sap Flow as a Measure of Transpiration

Measurements of sap flow are commonly used to indicate water use by plants and are reflective of the rate of transpiration (Burgess and Dawson, 2004; Dawson et al., 2007; Fisher et al., 2007). The heat ratio method (HRM) is one method of measuring sap flow that is capable of detecting low and reverse flow rates. The basic procedure entails the release of a heat pulse and measurement of a temperature increase ratio at two locations equidistant from the heat source (Figure 2; Burgess et al., 2001).

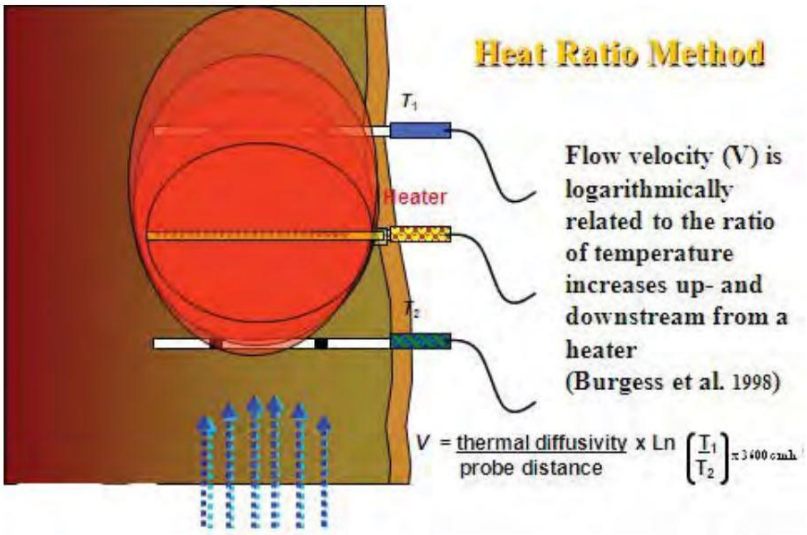

Figure 2: Diagram of the heat ratio method (HRM) used to measure sap flow in plants. T1 and T2 indicate temperature-detecting needles upstream and downstream of the heater needle. Blue dashed lines indicate typical direction of sap flow. Image copied from the SFM1 Sap Flow Meter Manual (Burgess and Downey, 2014).

The rate of evapotranspiration is generally controlled by the vapor pressure deficit (VPD), wind speed, and incoming solar radiation (Monteith, 1965). VPD is a function of temperature and relative humidity and is the primary driver of the water potential gradient between the atmosphere and soil. In humid climates, this water potential gradient

is weaker and may cause the VPD to have a lower correlation with transpiration rates (Monteith, 1965). Soil water is also regarded as a determining factor of transpiration rates because it is the source of water being moved along the water potential gradient. Therefore, transpiration cannot occur if soil water is inaccessible, regardless of climatic conditions (Fisher et al., 2007). This concept is supported by the soil-plant-atmosphere continuum model, which describes the movement of water by plants, from soil to the atmosphere. Once thought to be unidirectional, with water moving from soil to the atmosphere, it has recently been challenged with evidence of foliar and bark tissues absorbing water, causing the reversal of sap flow (Burgess and Dawson, 2004; Simonin et al., 2009; Eller et al., 2013).

Direct foliar uptake occurs when water droplets deposited on foliar surfaces are absorbed by moving across the leaf water potential gradient, the typical pathway being leaf cuticles. Due to this process, even leaf wetting events of low intensity or duration are capable of increasing plant water status. In the coast redwood forest, fog provides a low intensity wetting of leaves during the summer season. Species that do not directly absorb water still benefit from leaf wetting events, as it reduces water loss by evapotranspiration. Observed sap flow reversal can be indicative of tissues refilling, direct foliar uptake, and/or root efflux (Burgess et al., 2000). Direct foliar uptake is typically determined to be the cause of reverse sap flows in *S. sempervirens* trees during intense fog events.

It was typically assumed that transpiration is eliminated during the night hours due to stomatal closure driven by a lack of solar radiation and photosynthetic potential. Recent studies show that transpiration continues through the night in various ecosystems and plant species, which may be driven by refilling tissues and not strictly water loss

(Dawson et al., 2007; Fisher et al., 2007). Transpiration rates as high as 40% of the summer daytime maximum have occasionally been observed in a coast redwood forest on nights with high VPD (>3.0 kPa) and wind speeds (> 0.8 m/s) (Dawson et al., 2007). Nighttime transpiration is correlated with VPD, wind speed, and soil moisture to varying extents based on the climate and ecosystem studied (Fisher et al., 2007). High nightly transpiration rates in *S. sempervirens* are thought to be a result of uneven stomata, causing incomplete closure and/or poor responses to changes in the VPD (Burgess and Dawson, 2004). Because fog primarily begins at night, it is aids in reducing water loss in the coast redwood ecosystem by lowering the VPD, reducing nighttime transpiration, and supplying water to be directly absorbed by foliar and bark tissues.

4. METHODS

4.1 Study Location

The Caspar Creek Experimental Watersheds (CCEW; 39°21′N, 123°44′W) are located in northwestern California on the Jackson Demonstration State Forest in western Mendocino County (Figure 3). CCEW were established in 1961 by the U.S. Forest Service and California Department of Forestry and Fire Protection (CAL FIRE) as a joint study to examine the effects of timber management practices on streamflow and sedimentation. Studies have focused on tributaries of the North Fork (479 ha) and South Fork (417 ha), both of which are 4th-order channels. Historically, old-growth forests in the region were heavily logged from the 1860's until around 1904. After CCEW were established, second-growth forests in the South Fork were selectively harvested between 1971-1973 as part of the first major experiment. The second experiment involved

clearcutting sub-watersheds in the North Fork between 1985 and 1992. A third experimental harvest occurred in 2017 – 2019 which reduced stand densities in South Fork sub-watersheds to varying extents (Dymond et al., In Review).

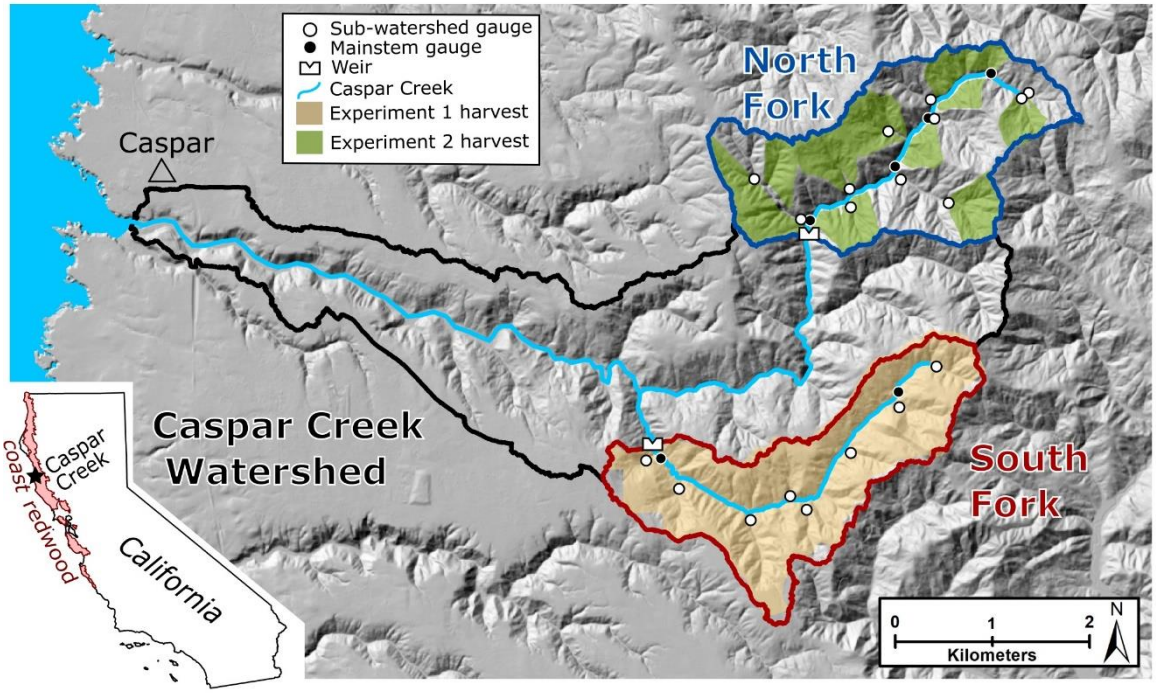

Figure 3: The Caspar Creek Experimental Watersheds (CCEW) and the surrounding region. Shading indicates relief in topography and timber harvest as part of the first (1971-1973) and second (1985-1992) experiments (Dymond et al., In Review).

The climate at CCEW is classified as Mediterranean, with wet, mild winters and relatively dry, cool summers. Low-intensity rainfall delivers 90% of annual precipitation between the months of October and April, with a mean annual depth of 1168 mm between the years of 1989 - 2018 (Dymond et al., In Review). The summers receive little precipitation but experience frequent fog events which develop at night, extend up to 16 km inland, and typically subside by midday. Located 7 km from the Pacific Ocean, temperatures at CCEW do not have large seasonal fluctuations due to the coastal

influence. Mean monthly air temperatures fall between 6.7 – 15.6°C. Geologically, CCEW are underlain by marine sandstone and shale that developed into marine terraces which were deeply incised by streams. This deep incision created steep slopes that frequently exceed 50%. Elevations in the watersheds range between 37 and 320 m. Soils at CCEW developed from the weathering of marine sandstone to produce well-draining clay loams in the Ultisol and Alfisol soil orders (Henry, 1998). The Vandamme and Irmulco-Tramway soil series compose 90% of the soils found in the watersheds (Table 1). The dominant tree species at CCEW are coast redwood (*Sequoia sempervirens* (D. Don) Endl.) and Douglas fir (*Pseudotsuga menziesii* (Mirb.) Franco). Also present but in lower quantities are grand fir (*Abies grandis* (Dougl. ex D.Don) Lindl.), western hemlock (*Tsuga heterophylla* (Raf.) Sarg.), tanoak (*Lithocarpus densiflorus* (Fook. and Arn.) Rohn), and red alder (*Alnus rubus* Bong.) (Cafferata and Reid, 2013). Understory vegetation includes evergreen huckleberry (*Vaccinum ovatum* Pursh), Pacific rhododendron (*Rhododendron macrophyllum* D. Don), and sword fern (*Polystichum munitum* (Kaulf.) Presl.) (Henry, 1998).

Table 1: Soil order, series, subgroup, and respective descriptions of soils commonly found in the Caspar Creek Experimental Watersheds (National Cooperative Soil Survey, 2020).

Soil Order	Soil Series	Soil Subgroup	Description
Ultisol	Vandamme	Typic Haplohumults	Typical Ultisols with organic matter present and minimum horizon development
Alfisol	Irmulco-Tramway	Ultic Hapludalfs	Old/developed Alfisols in humid environment with minimum horizon development

The third major experiment is implementing varying degrees of stand density reduction in the South Fork of CCEW using current California Forest Practice Rules. The Williams watershed is serving as one of the controls with no harvest. Mean stand density in Ziemer watershed was reduced by 76%, serving as the highest reduction rate of the third experiment (Figure 4). Both watersheds have established 1/20th hectare study plots along a hillslope transect as part of the Plant-Soil-Water Dynamics Study (Dymond et al., In Review). These study plots are numbered based on their position along the hillslope, ranging from 1 (riparian) to 5 (ridge) (Figure 5).

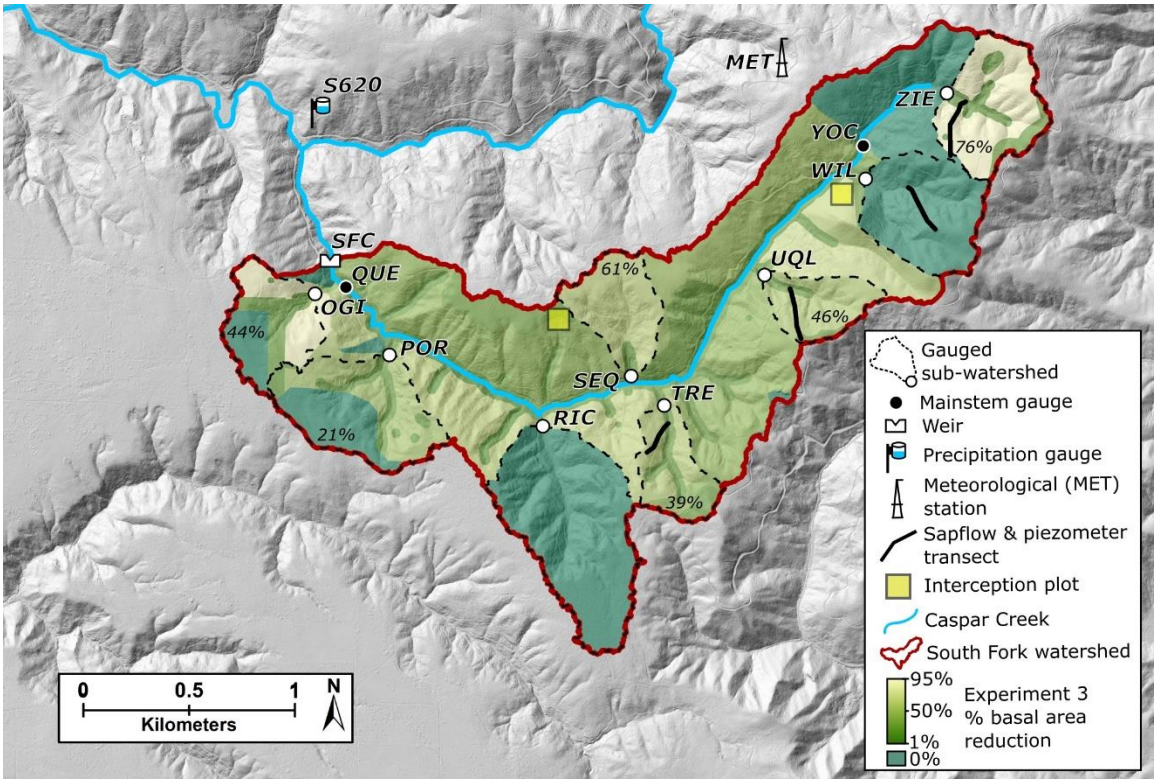

Figure 4: Basal area reduction in the South Fork Caspar Creek as part of the third experiment (Dymond et al., In Review).

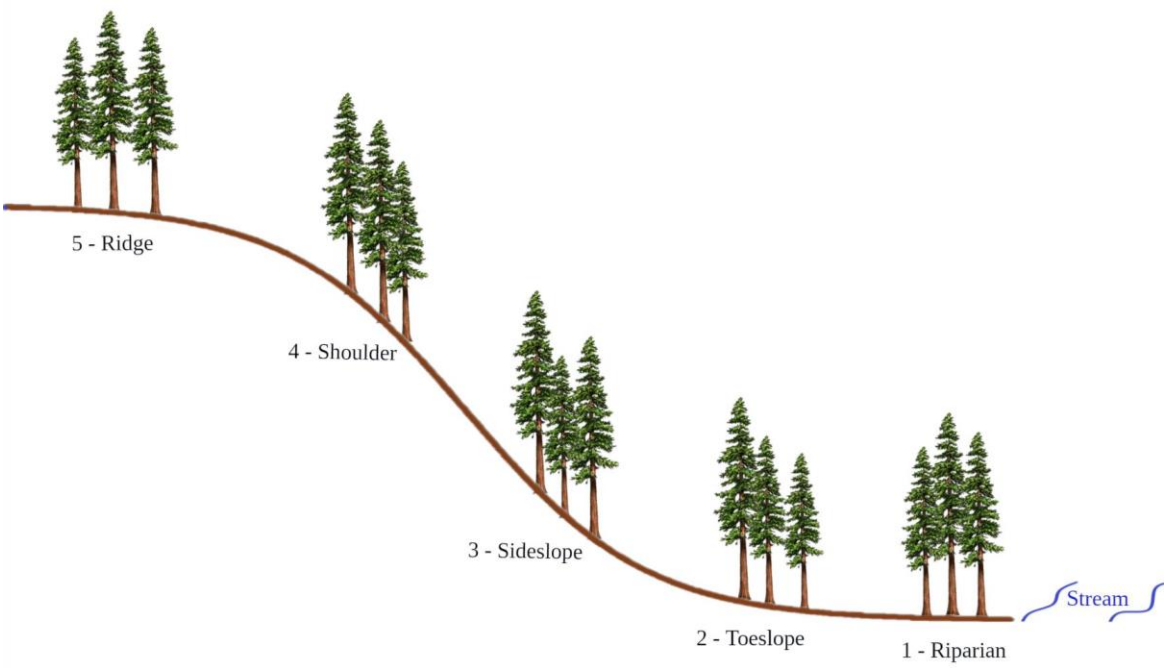

Figure 5: Schematic of study plots established along a hillslope transect as part of the Plant-Soil-Water Study (Dymond et al., In Review).

4.2 Study Plot Description

Prior field observations indicated that most fog drip occurs near the top of the ridges at CCEW. Given these observations, shoulder and ridge sites were instrumented in each sub-watershed to study fog interception; four sites were included in this study. Physical site characteristics and overstory species distribution at study sites were measured in 2019 (Table 2). As part of a Plant-Soil-Water Dynamics Study, soil moisture (15 cm, 30 cm, 100 cm), groundwater, temperature, relative humidity, photosynthetically active radiation (PAR), and sap flow were measured at each plot (Dymond et al., In Review). A nearby meteorological station (MET1) recorded precipitation and visibility over the course of the study (Figure 6). Precipitation was recorded using an unshielded OTT

Pluvio N weighing rain gauge (Ott HydroMet, Kempten, Germany) with a resolution of 0.025 mm. Visibility was recorded by a CS120A Visibility Sensor (Campbell Scientific Inc., Logan, UT, USA), capable of detecting reduced visibility down to 5 meters.

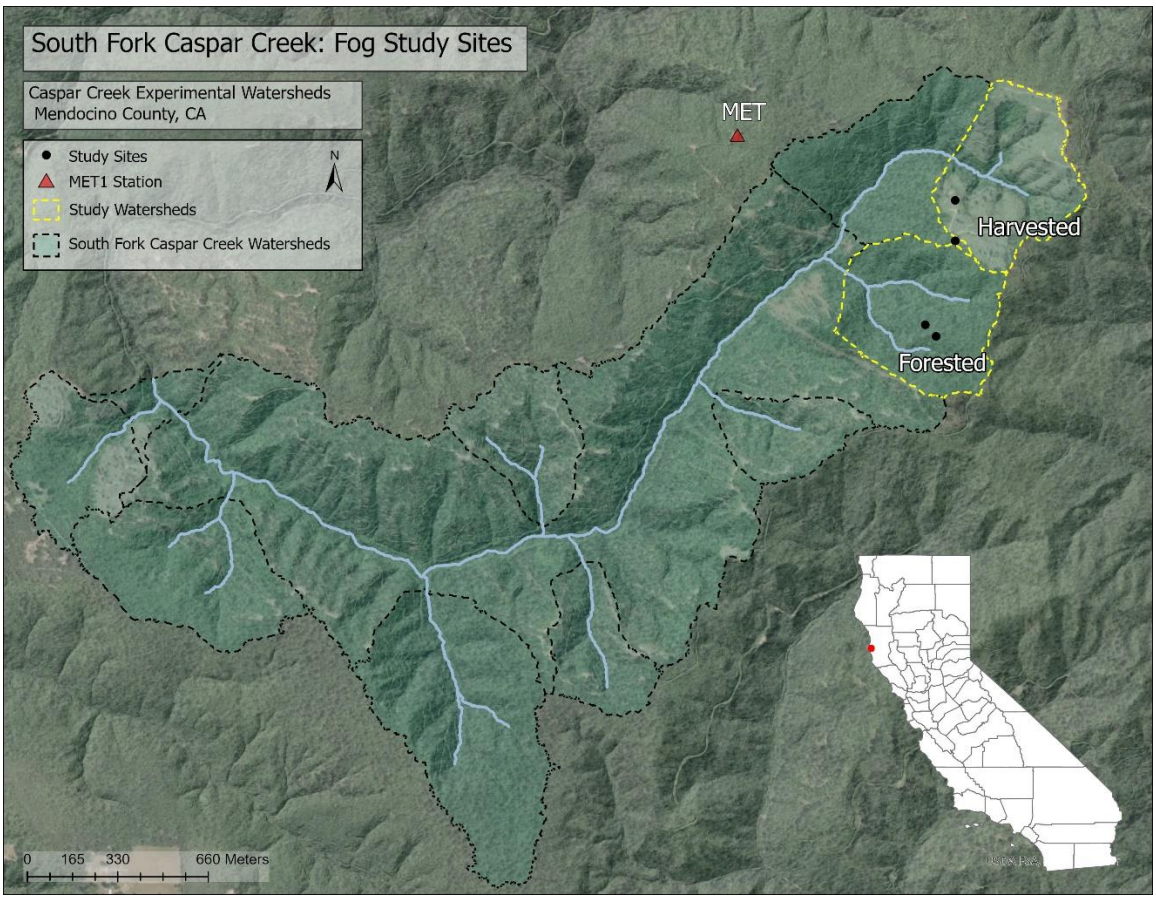

Figure 6: Map of South Fork Caspar Creek watersheds (yellow polygons) and study sites (black points) included in this study. Meteorological station (MET1) is also displayed (red triangle).

Table 2: Physical characteristics and overstory species distribution of study sites. Species acronyms refer to coast redwood (RW), tan oak (TO), Douglas fir (DF), grand fir (GF), and rhododendron (RD).

Treatment		**Forested**		**Harvested**	
Position		**Shoulder**	**Ridge**	**Shoulder**	**Ridge**
Physical Characteristics	Elevation (m)	251.5	274	248	270
	Aspect (°)	357	288	351	294
	Slope (%)	55	25	28	19
	Basal Area (m^2/ha)	32	20	2	6
Species Distribution (% of Total Basal Area)	RW	27.9	87.4	84.2	83.5
	TO	0.3	1.2	15.8	16.4
	DF	69.9	4.1	0	0
	GF	0.8	4.3	0	0
	RD	1	3	0	0

Additional sensors were installed in Spring 2020 at each site (Table 3). Soil moisture sensors were placed between the bole and the drip-edge of a study tree ("bole"), at the canopy drip-edge ("drip"), and in a nearby opening ("open"). In order to capture meteorological conditions during fog interception, one wind speed and direction sensor, one temperature and relative humidity sensor, and one leaf wetness sensor was mounted in a canopy location (Table 3). A second leaf wetness sensor was placed in the litter layer near the canopy drip edge of a study tree to measure increases in litter moisture (Figure 7).

Table 3: Sensors installed at each study site in addition to the instrumentation that was already present as part of the Plant-Soil-Water Dynamics Study (Dymond et al., In Review). CSI refers to the Campbell Scientific, Inc. manufacturer (Logan, UT, USA).

Sensor Name (Manufacturer)	Quantity (per plot)	Description
SoilVUE10 (CSI)	3	1-meter long soil moisture sensor
LWS (CSI)	2	Leaf wetness sensor
03002 Wind Sentry Set (R.M. Young)	1	Measuring wind speed and direction
EE181 (CSI)	1	Measuring temperature and relative humidity
CR1000 (CSI)	1	Data logger

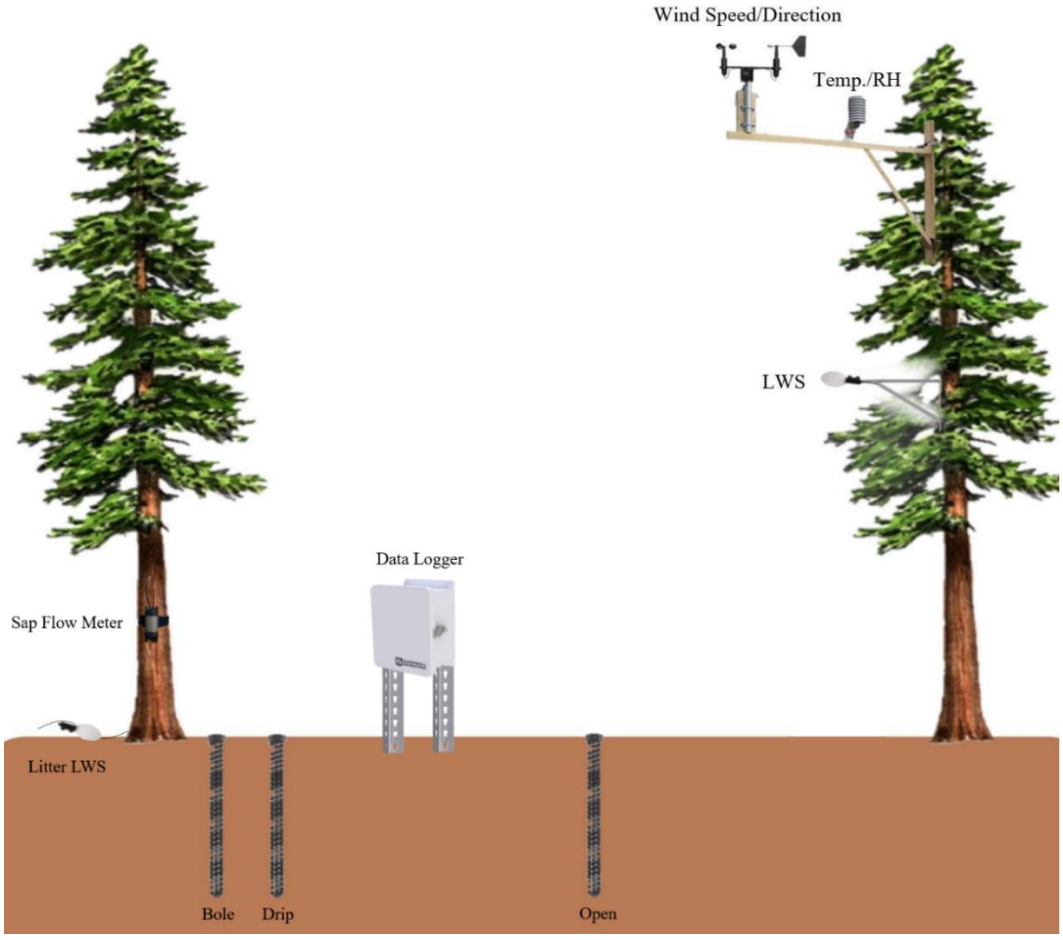

Figure 7: Schematic of the general layout of sensors at each study site (not to scale).

4.3 Soil Moisture Sensors

Sensor installation began in March 2020 and included three soil moisture sensors and one data logger with enclosure at each study plot. Appendix A contains detailed instructions and a checklist that was used for the installation of ground and canopy sensors at each site. Plot centers established from the Plant-Soil-Water Dynamics study were used in this study. The harvested ridge site bordered a forested watershed to the west, so an easterly azimuth (60 – 110°) was used to avoid possible edge effects. The remaining three sites were installed at the same azimuth and side-slope of the plot center. Areas of compaction and unique drainage features were avoided to ensure representative soil conditions.

The 1-m long Campbell Scientific SoilVUE10 sensors (Logan, Utah, USA) were programmed to record soil volumetric water content (VWC) every 15 minutes. To measure episodic and seasonal changes in soil moisture, VWC at each of the four study sites was recorded at 5, 10, 20, 30, 50, 100 cm depth. One soil moisture sensor was placed within 1 meter of the bole of the *S. sempervirens* sap flow tree at the plot center ("bole"). "Drip" soil moisture sensor was placed at the canopy drip-edge of the sap flow tree and "open" soil moisture sensor in a nearby opening. Openings at the forested sites were difficult to find, so the best suitable location for the "open" sensor was one with a gap in canopy cover. Nearby understory vegetation was also trimmed to expand openings at these sites. Data were recorded using a CR1000 (Campbell Scientific Inc., Logan, UT, USA).

4.4 Canopy Sensors

In order to measure wind conditions experienced by the canopy at CCEW, one wind speed and direction sensor (03002 R.M. Young Wind Sentry Set, Campbell Scientific Inc., Logan, UT, USA) was installed within the canopy at each study site. A temperature and relative humidity sensor (EE181, Campbell Scientific Inc., Logan, UT, USA) housed in a radiation shield (RAD10E, Campbell Scientific Inc., Logan, UT, USA) was also installed within the canopy at each study site. The wind speed and direction and temperature and relative humidity sensors were secured to a mounting frame (Figure 8) at an azimuth of ~ 315°. This orientation was chosen to face the prevailing north-northwesterly summer winds in this region (Williams, 2009; Rastogi et al, 2016). The availability and climbing safety of trees near study plot centers dictated the chosen location for canopy sensor deployment.

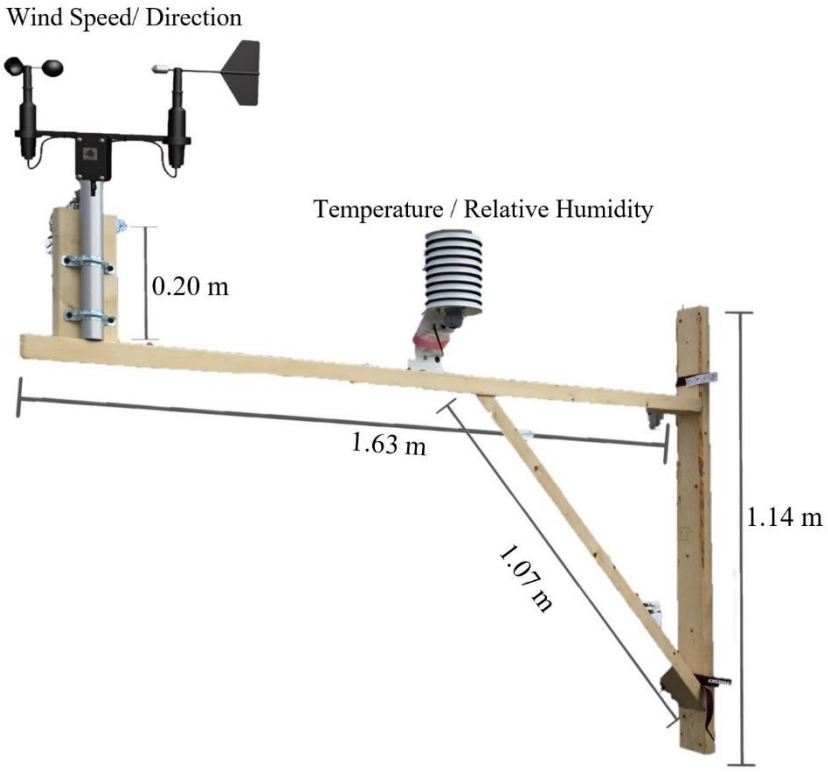

Figure 8: Dimensions of platform for mounting wind speed, wind direction, temperature, and relative humidity sensors in a canopy location. Figure is not to scale.

The Campbell Scientific LWS (Logan, Utah, USA) leaf wetness sensor measures the dielectric constant of a zone approximately 1 cm from the upper surface of the sensor. Since the dielectric constant of water (~80) is significantly different from air (~1), measurements taken by the sensor indicate the presence of water on or near the surface. The output generated by the LWS is a millivolt (mV) signal proportional to the amount of water on the sensor surface and is therefore capable of indicating the presence of rain or fog. Manufacturer instructions recommend setting a threshold at 280 mV, indicating anything below this value reflects a dry sensor.

A LWS was mounted to a separate mounting frame and secured to a tree at a height of 6.1 meters (20 feet). This height was determined by a limiting cable length on this sensor, with a maximum available length of 20.1 meters (66 feet). At the two shoulder sites, the LWS was installed on *P. menziesii* trees that held the other canopy sensors. At the harvested ridge site, the LWS was installed on the same *S. sempervirens* tree as the wind and temperature / relative humidity sensors. Due to length limitation and site obstructions at the forested ridge site, the LWS was installed on a separate *S. sempervirens* tree than the wind, temperature, and relative humidity sensors. An L-bracket was secured to the bole of a tree using ratchet straps and oriented to point in a northwesterly direction (azimuth of ~ 315°). The LWS was secured to the end of the bracket by cable ties and tilted ~15° to facilitate drainage (Figure 9).

Figure 9: Photograph of leaf wetness sensor (LWS) secured to a bracket and mounted at a height of 6.1 meters (20 feet) in a *S. sempervirens* tree at the harvested ridge study site.

4.5 Monitoring Litter Moisture

Moisture levels of the litter layer were measured to determine possible fog drip inputs that were intercepted before reaching the mineral soil. The litter layer is characterized as all dead, partially decomposed, fresh, or dry plant matter that is above the mineral soil surface (Law et al., 2008). The litter layer can be broken into several sub-layers consisting of the O_a, O_e, and O_i layers. The O_a layer contains identifiable plant matter (e.g., twigs, leaves, needles), the O_e is partially broken-down material, and the O_i is fully decomposed and unidentifiable organic matter. A gravimetric method and leaf wetness sensor were used to measure litter moisture. The gravimetric method determines the portion of water within a sample by recording the sample weight before and after oven drying. Collected litter samples consisted primarily of the O_a and O_e layers due to low development of the O_i organic layer, which was found only in certain locations at the forested ridge site.

Sampling of the litter layer was conducted approximately every three days between mid-July and mid-August of the 2020 summer fog season. All samples were collected in the morning, between 07:00 and 12:00 PST (i.e., UTC-08:00) to avoid evaporation losses. Four samples were collected at each study site, one sample in each cardinal direction from the plot center, to account for variability within the study plot. All samples were collected within six meters of the plot center. A random distance (0-6 m) for each sample was determined using a random number generator, but often required slight adjustment to avoid trails, trees, and equipment. Approximately 15 grams of litter was collected into an airtight Ziploc bag, including all litter down to the mineral soil. Thick layers of organic matter (i.e., fully decomposed material) and sticks greater than

four mm in diameter were excluded from the sample (Law et al., 2008). Samples were stored in a cool, dry location until processed, which generally occurred within several hours of collection.

Laboratory processing involved transferring ~15 to 25 g of litter to a metal tin of known weight and recording the wet weight of the sample. These samples were then placed in an oven at 105 °C for at least 48 hours to ensure all water evaporated (Schunk et al., 2016). Dry samples removed from the oven and were weighed within five minutes of removal. Calculation of litter gravimetric water content (GWC) was done using the following equation:

$$GWC\ (\%) = \frac{(M_W - M_D)}{M_D} * 100 \qquad \textit{(Equation 1)}$$

Where M_W is the weight of the sample before drying ("wet"), and M_D is the dry weight of the sample. The four samples collected at a study site on one sampling day were averaged.

LWS can also be used as an indicator of water inputs to the litter layer. Increases in the LWS output are found to have a strong, positive relationship with water content and the orientation of the sensor determines its contact with the surrounding litter layer. An insertion angle of 45° generally ensures the most contact without pooling water on the sensor surface (Acharya et al., 2017). The LWS was inserted into the litter at an angle approximately 45° to the ground surface using a digital clinometer as a guide (Figure 10). Sensors were placed within two meters of the *S. sempervirens* sap flow study tree, with an undisturbed litter layer at least five centimeters thick. Due to site and cable constraints, the azimuths of the LWS in relation to the study tree varied across sites (Table 4). The

ground slope and litter depth at the location of the litter LWS sensor also varied among sites. Installation of the litter LWS was completed on July 11, 2020.

Table 4: Ground slope (degrees), litter depth (cm), and azimuth of LWS installed in litter layer at each study site.

Study Site	Slope (°)	Litter Depth (cm)	Azimuth (º)
Forested shoulder	29	8	120
Forested ridge	20	7	230
Harvested shoulder	16	5	310
Harvested ridge	17	9	212

Figure 10: Installation of LWS to litter layer at a 45° angle to the ground slope using a digital clinometer.

4.6 Sap Flow Meters

Installation of SFM1 Sap Flow Meter (ICT International Pty Ltd, Armidale, Australia) was done as part of the Plant-Soil-Water Dynamics study (Dymond et al., *In Review*). The SFM1 meter measures sap flow velocity using the HRM and can estimate

sap flow volumes with specified cross-sectional measurements of the study tree. The HRM technique was chosen due to its ability to detect both zero-flow and reverse sap flow. Installation of sap flow meters at my sites was completed in 2016. Sap flow meter installation and measurements of tree characteristics followed protocol outlined by the SFM1 Sap Flow Meter Manual (Burgess and Downey, 2014). Sensors were installed at the tree diameter at a height of 1.37 m of one *S. sempervirens* tree located at the center of each study plot. Study trees selected were of a similar diameter class, ranging from 31.7 cm to 41.9 cm at the time of installation.

4.7 Analysis

4.7.1 Climate

General climate trends were summarized using observations recorded at the MET1 meteorological station. Precipitation volumes recorded every ten minutes were summed to determine daily totals over the hydrologic year 2020 (Aug. 1, 2019 – Aug. 1, 2020). To differentiate water deposition caused by precipitation versus fog drip, a threshold recorded by the rain gauge was set to one mm per day; values below this threshold were assumed to be caused by excessive fog drip. The CS120A Visibility Sensor at the MET1 meteorological station also recorded visibility conditions every ten minutes. Following the technical definition of fog, visibility reduced by one km in the absence of rainfall was used to indicate fog presence. Ten-minute observations were summarized showing the percentage of each day with reduced visibility, indicating extent of fog presence. As wildfires late in the summer season impacted air quality near Caspar Creek, days with reduced air quality during wildfires were noted to determine the impact

on visibility readings. Specific dates were determined by field observations and AirNow reports of daily air quality index, measured at a Fort Bragg station (U.S. EPA, 2020).

4.7.2 Leaf Wetness as Indicator of Fog Deposition

Hourly measurements of leaf wetness, recorded as mV by the LWS, were transformed into a binary code to indicate whether the sensor was wet or dry using the 280-mV threshold. Fog was presumed to be present when the LWS was wet and there was no significant daily precipitation (> 1 mm) recorded by the MET1 rain gauge. Hourly readings of leaf wetness were averaged over each day as well as over the entire summer fog season (June – September) for each study site. The fog season defined in this study begins on June 4th due to missing data at both shoulder sites prior to this date. A "fog day" was defined as a day that recorded at least 8 hours of leaf wetness and no significant precipitation at the MET1 station (< 1 mm). The number of fog days at each study site were summed over each month of the fog season (June - September). To compare the relative frequency of fog between months, fog days were reported as a percentage of total days in each month.

An analysis of variance (ANOVA) was conducted to assess whether fog presence varied by study site ($\alpha = 0.05$). If the ANOVA output indicated differences were present, sites were compared to one another using Tukey's Honestly Significant Differences (HSD) post-hoc test using the agricolae package (Mendiburu, 2020) in R version 4.0.2 (R Core Development Team, 2020).

The mean seasonal leaf wetness caused by fog deposition was compared between sites using Welch's two-sample t-test, which corrects for unequal variances. Due to the

nature of time series data, observations cannot be assumed to be independent of one another. This was addressed by computing an effective sample size and adjusting significance values using the following formula:

$$N_{eff} = \frac{N}{\frac{(1+\rho)}{(1-\rho)}} \qquad \textit{(Equation 2)}$$

Where N_{eff} is the effective sample size, N is the original, autocorrelated sample size and ρ is the first-order autocorrelation coefficient of the dataset (Pennsylvania State University, 2018). This approach is statistically robust due to its high penalty for autocorrelation, assuming the number of independent observations to be much lower than the original length of observations (Fuller, 1996). Results from the adjusted Welch's two-sample t-test were used to corroborate significant differences determined by Tukey's HSD test, which does not account for autocorrelation.

4.7.3 Fog Deposition and Meteorological Variables

To determine possible relationships between fog deposition and varying climatic conditions, a cross correlation lag analysis was performed to evaluate whether any climatic factors cause or respond to fog (Cárdenas et al., 2017). This analysis examines the correlation between response variables (y_t), and different time shifts in predictor variables (x_{t+k}). Lag correlation was evaluated at the hourly temporal resolution. The response variable analyzed was fog deposition, measured as mV by the LWS. Predictor variables were mean wind speed, mean air temperature, maximum vapor pressure deficit (VPD), maximum relative humidity (RH), and photosynthetically active radiation (PAR). VPD was calculated at each study site using the following formula:

$$e_s = 611 * \frac{\exp(17.27 * T_a)}{(T_a + 237.3)} \quad \textit{(Equation 3)}$$

Where e_s is the saturation vapor pressure in Pascal (Pa), T_a is the air temperature (°C). The actual vapor pressure was calculated using the minimum hourly relative humidity observations in the following formula:

$$e_{a_{min}} = e_s * \frac{RH_{min}}{100} \quad \textit{(Equation 4)}$$

Where $e_{a\ min}$ is the minimum actual vapor pressure (Pa), e_s is the saturation vapor pressure (Pa), and RH_{min} is the minimum hourly relative humidity (%). The minimum e_a was used to get the hourly maximum VPD, using the following formula:

$$VPD_{Max} = \frac{(e_s - e_{a_{min}})}{1000} \quad \textit{(Equation 5)}$$

Where VPD_{Max} is the maximum VPD (kPa), e_s is the saturation vapor pressure (Pa), and $e_{a\ min}$ is the minimum actual vapor pressure (Pa). RH is dependent on temperature, and VPD was derived from temperature and RH; therefore, it is important to note that these variables were not independent of one another. The lag period was used to indicate whether a meteorological variable was influencing the change in fog deposition (negative lag) or was responding to it (positive lag). Four days with fog presence observed at all study sites were selected to run the cross-correlation analysis: June 23, July 20, July 30, and August 21. Each selected fog day and site was analyzed independently, beginning at 18:00 on the selected day and ending the following day at 18:00 to capture the entirety of the fog event. The highest cross correlation coefficient between fog deposition and each meteorological variable within a 95% confidence interval at each site was selected for comparison.

4.7.4 Soil Moisture

Mean daily volumetric water content (VWC) was converted from cm^3/cm^3 to percent VWC and evaluated at a daily temporal resolution. The influence of fog drip on soil moisture was evaluated at the upper ten centimeters of soil. Deep soil water was summarized by averaging the VWC of soils at 100 cm depth at the bole and drip edge positions. These two sensors were chosen based on their proximity to the study tree; the opening soil moisture sensor was located the farthest from the study tree and displayed different VWC of deep soils than the bole and drip edge sensors. To remove seasonal effects and better visualize changes in soil moisture, daily changes were calculated on mean daily VWC at each site and sensor position.

4.7.5 Litter Moisture

Summary statistics (mean, s) were completed on gravimetric water content (GWC) across each sample period. The mean seasonal GWC of litter was compared for each site combination using Welch's two sample t-test ($\alpha = 0.05$) with adjusted degrees of freedom (Equation 2).

4.7.6 Sap Flow Velocity

Transpiration rates were determined by 10-minute measurements of sap flow velocity recorded by the SFM1 Sap Flow Meters. Raw observations were processed in SFT1 Sap Flow Tool software (v1.5, ICT International Pty Ltd, Armidale, Australia) and corrected with site-specific wood properties to account for wounding associated with sensor installation (Burgess and Downey, 2014). Corrected data were exported and further analyzed in R version 4.0.2. Sap flow velocity measurements were standardized to

allow for comparison between sites. A “true zero” value of sap flow is typically determined by cutting the study tree; this could not be done due to the destructive nature of the process and the need to continue sap flow measurements beyond this study. Instead, observations were standardized by representing the sap flow velocity as a percentage of the seasonal maximum recorded at each respective tree (Dawson et al., 2007; Eller et al., 2013; Burgess and Dawson, 2004). The seasonal maximum was defined as the maximum sap flow velocity between the months of May - September.

To better understand transpiration rates during peak fog presence, sap flow observations were examined during night hours. Hourly observations between 00:00 and 08:00 were characterized as “nightly” and transpiration was assumed independent of photosynthetic activity, which typically begins with increased solar radiation. Although the early morning hours (06:00 – 08:00) are around the time of sunrise, these hours frequently reported the lowest sap flow rates found over the course of the day. To examine the relative differences in transpiration rates between nights with fog presence and fog absence, summary statistics (mean, standard deviation, minimum, and maximum) were compared. Fog presence was characterized by leaf wetness readings; if the LWS reported values above the “dry threshold” (280 mV) with no significant precipitation (< 1mm/day), fog was presumed to be present.

Hourly observations of sap flow velocity were aggregated to a daily temporal resolution to remove diurnal fluctuations. Summary statistics (mean and standard deviation) of sap flow over the summer season (June – Sept.) were determined for each site and compared using Tukey’s HSD test. Hourly observations of sap flow velocity (represented as % of seasonal maximum) below zero were assumed to indicate sap flow

reversal and direct foliar uptake. These negative sap flow readings were summarized over the summer season to indicate the proportion of time that each site had reverse sap flow.

Due to variation based on site-specific characteristics and lack of replicates in this study, statistical analysis was performed on each study site independently. Relationships between hourly sap flow velocity and climatic factors (e.g., VPD, PAR, wind speed, leaf wetness) at each site were determined using the Kendall tau-b correlation coefficient (Kendall, 1938). Kendall correlation is a nonparametric, rank-based test used to determine the strength and direction of association between two variables. This test is a conservative correlation method capable of handling tied ranks and nonlinear relationships, unlike the Spearman's rho and Person's r correlation methods. Because hourly observations were used for each site and climatic factor, the number of observations were generally between 2100 and 2800. The only exception occurred for the PAR variable at the harvested ridge site, where missing data brought the number of observations down to 1075.

5. RESULTS

5.1 Climate over the Summer 2020 Season

Over hydrologic year 2020 (Aug. 1, 2019 – Aug. 1, 2020), total precipitation recorded at the MET1 station was 704 mm, only about 60% of the annual average. The last significant precipitation event before the summer fog season was on May 30th, recording 3.25 mm of rainfall. Over the following months, minor precipitation volumes were recorded and correlated with fog events. Using the one mm threshold, only one

precipitation event occurred over the summer fog season, when 1.09 mm fell on Sept. 24th (Figure 11a).

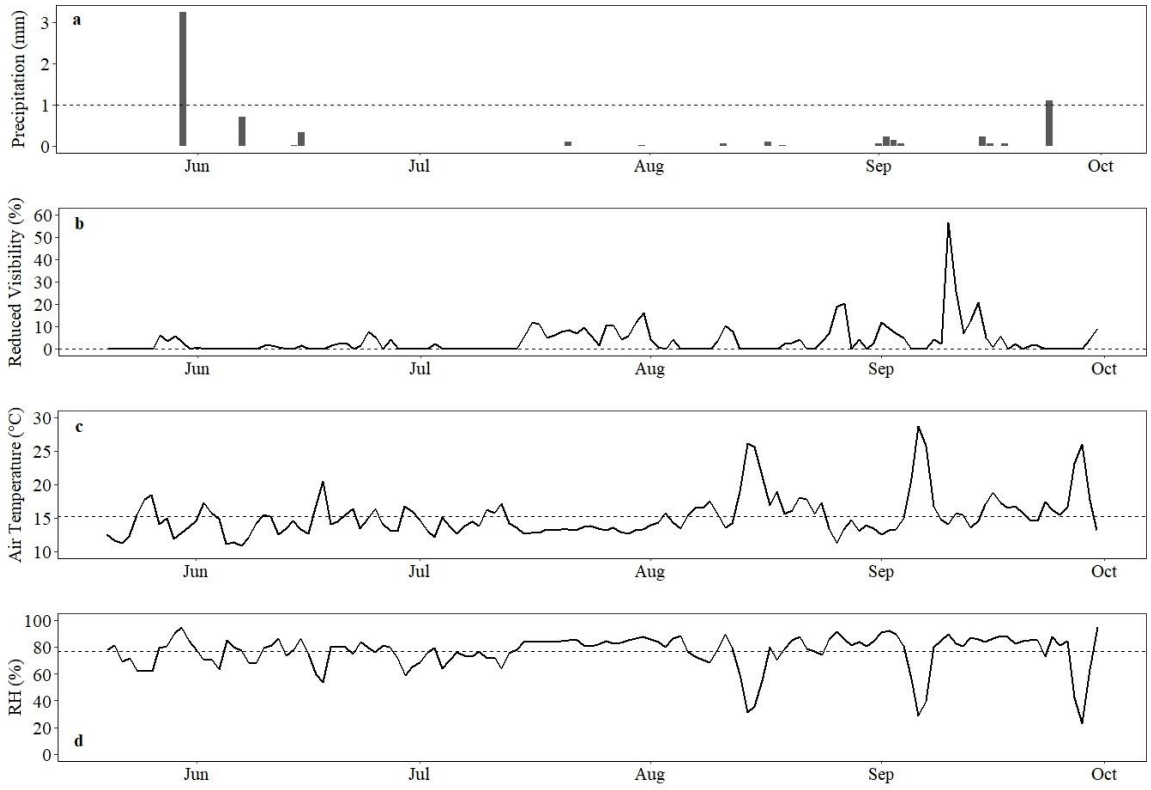

Figure 11: Climate data recorded at the MET1 meteorological station from May 20-Sept. 30, 2020. (a) Daily precipitation (mm), dashed line indicating 1-mm threshold used to determine precipitation event. (b) Percent of day with reduced visibility (%), dashed line at zero indicates no reduction in visibility. (c) Mean daily air temperature (°C), dashed line indicating mean summer value of 15.25 °C in 2020. (d) Relative humidity (RH, %), dashed line indicating mean summer RH of 76.5% in 2020.

Visibility data over the summer fog season indicated that June and beginning of July did not experience frequent fog events (Figure 11b). Reduced visibility that did occur during this period generally lasted less than 10% of the day. Beginning in mid-July, reduced visibility indicated a prolonged foggy period that lasted until the beginning of

August. Fog events increased in duration in late August and September and caused visibility to be reduced up to 20% of a day. In mid-September, reduced visibility peaked over 55% of the day, but this was presumed to be caused by wildfire smoke rather than fog. Wildfires in California began in August 2020 and marked the largest wildfire season recorded in the state's recent history, with over four million acres burned (CAL FIRE, 2020). Between September 9th-14th, Fort Bragg recorded impacted air quality caused by wildfires and field observations indicated ash falling from the sky (U.S. EPA, 2020).

The daily average temperature over the 2020 summer fog season was 15.25 °C. Maximum temperatures of 29 °C and 26 °C were recorded on Sept. 6th and August 14th, respectively (Figure 11c). Ten-minute observations of relative humidity never exceeded 96% at the MET1 station, even during the May and September precipitation events. Overall, the mean daily relative humidity was 76.5% over the summer fog season (Figure 11d).

5.2 Spatial and Temporal Trends of Fog

The distribution of fog days varied across study sites and summer months of the fog season (Figure 12). The forested ridge study site consistently reported the lowest number of fog days each month of the season. July had the highest number of fog days at all sites except for the forested shoulder. At the harvested shoulder site, every day in the month of July was a fog day. Fog presence in September was the most similar across all sites except for forested ridge, which again had fewer fog days than the other sites (Figure 12).

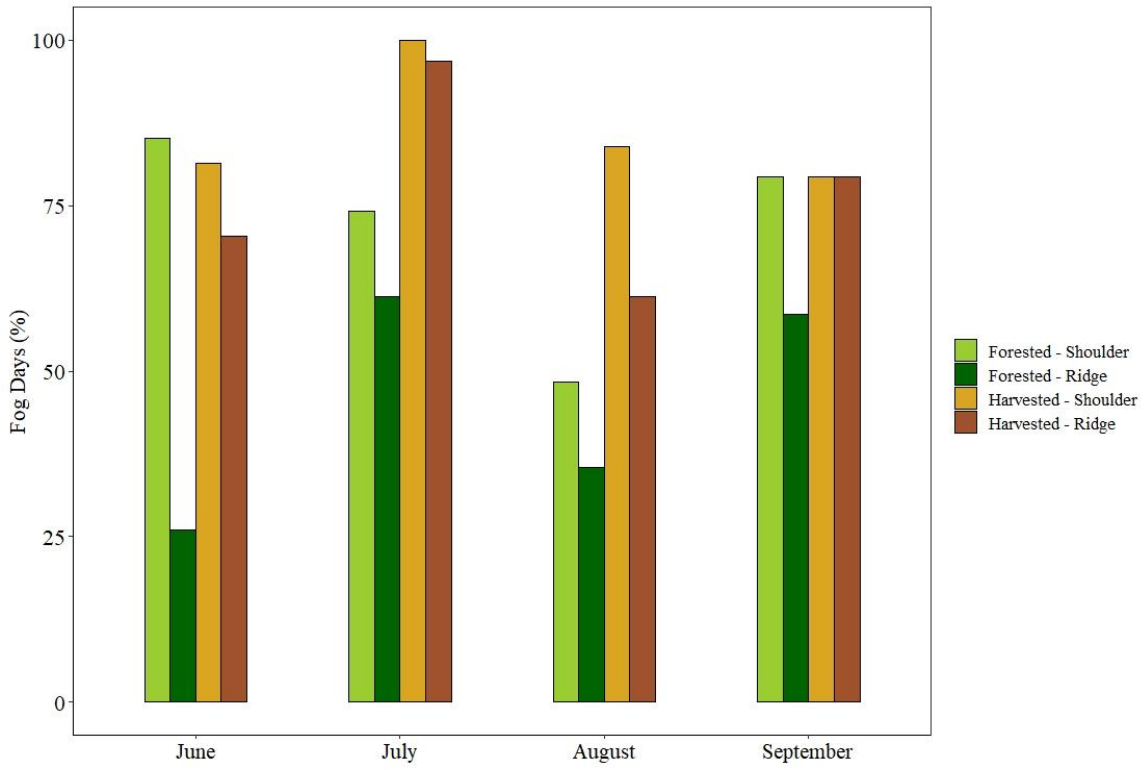

Figure 12: The percentage of fog days at each study site recorded by leaf wetness sensors from June-September 2020.

Fog deposition also varied across study sites over the summer fog season, as measured by the degree of leaf wetness. Shoulder sites in both the harvested and forested treatments generally recorded the highest degrees of fog deposition between June and mid-August, with the highest peaks occurring in July (Figure 13). However, beginning in late August, the forested ridge site began to record fog deposition similar to the two shoulder sites, while the harvested ridge site continued to report lower leaf wetness values. Results of the two-sample Welch's t-test showed significant differences between the shoulder and ridge positions, with no differences between harvested and forested sites ($\alpha = 0.05$). Further comparison of the means by Tukey's HSD test supported this result,

indicating that fog deposition was similar across study sites based on their topographic position and there were no differences between treatments (Table 5). Because both tests indicated the same results, only the results of Tukey's HSD are presented for subsequent analyses, additional tables of t-test results can be found in Appendix C.

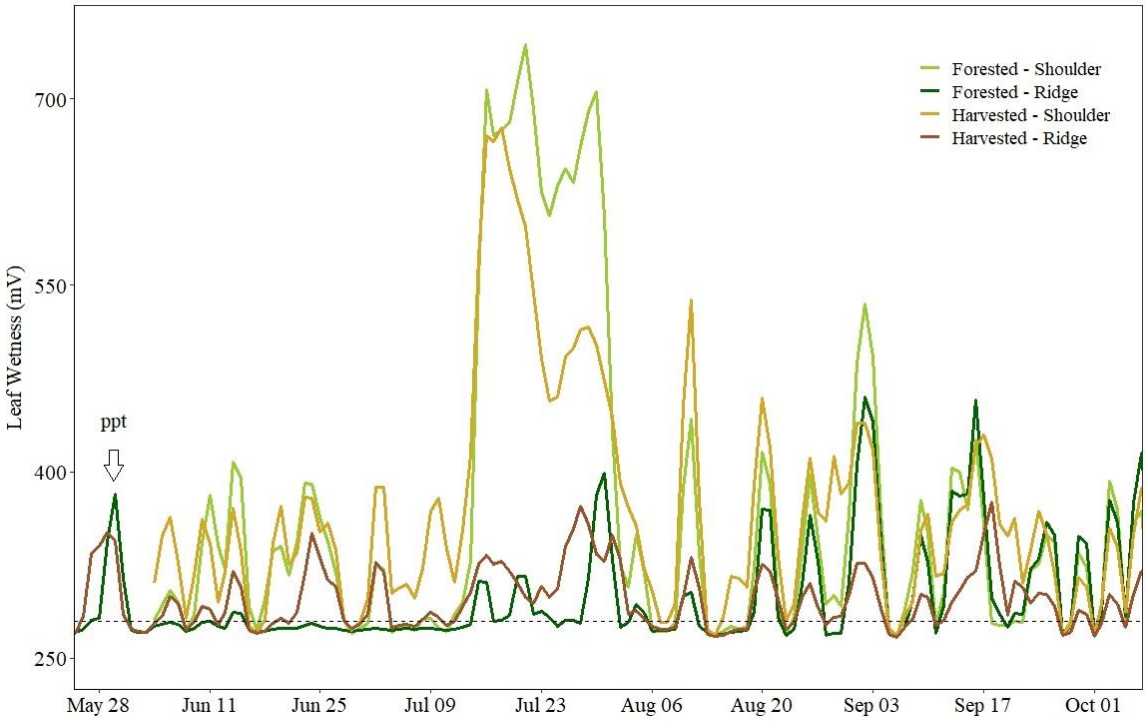

Figure 13: Deposition of fog at each study site over the summer season, as recorded by the leaf wetness sensor (mV). Lines represent the mean daily mV signal, with a 2-day moving average applied to display the general trends. Dashed line at 280 mV represents the "wet" threshold. One precipitation event on May 30th is labeled as "ppt." Data collection began on March 13, 2020 at the forested ridge and harvested ridge sites. Data collection at both shoulder sites began on June 04, 2020.

Table 5: Mean, standard deviation (s), and Tukey's HSD results ($\alpha = 0.05$) of daily leaf wetness (mV) over the summer fog season (June - September). Sites that share a Tukey's HSD group have similar letters.

Site	**Mean (mV)**	**s (mV)**	**Tukey's HSD Group**
Forested - Shoulder	372	137.6	a
Forested - Ridge	298	52.4	b
Harvested - Shoulder	373	99.8	a
Harvested - Ridge	298	29.2	b

General diurnal trends in leaf wetness indicated that fog was present in the evening as solar radiation decreased and dissipated as radiation increased over the course of the day (Figure 14). The VPD also followed a diurnal trend, generally reaching zero when leaf wetness was at its highest. Over the summer fog season, the harvested shoulder, harvested ridge, and forested shoulder sites had fog present an average of 13 hours per day, and the forested ridge site had fog present an average of 7 hours per day (Figure 15).

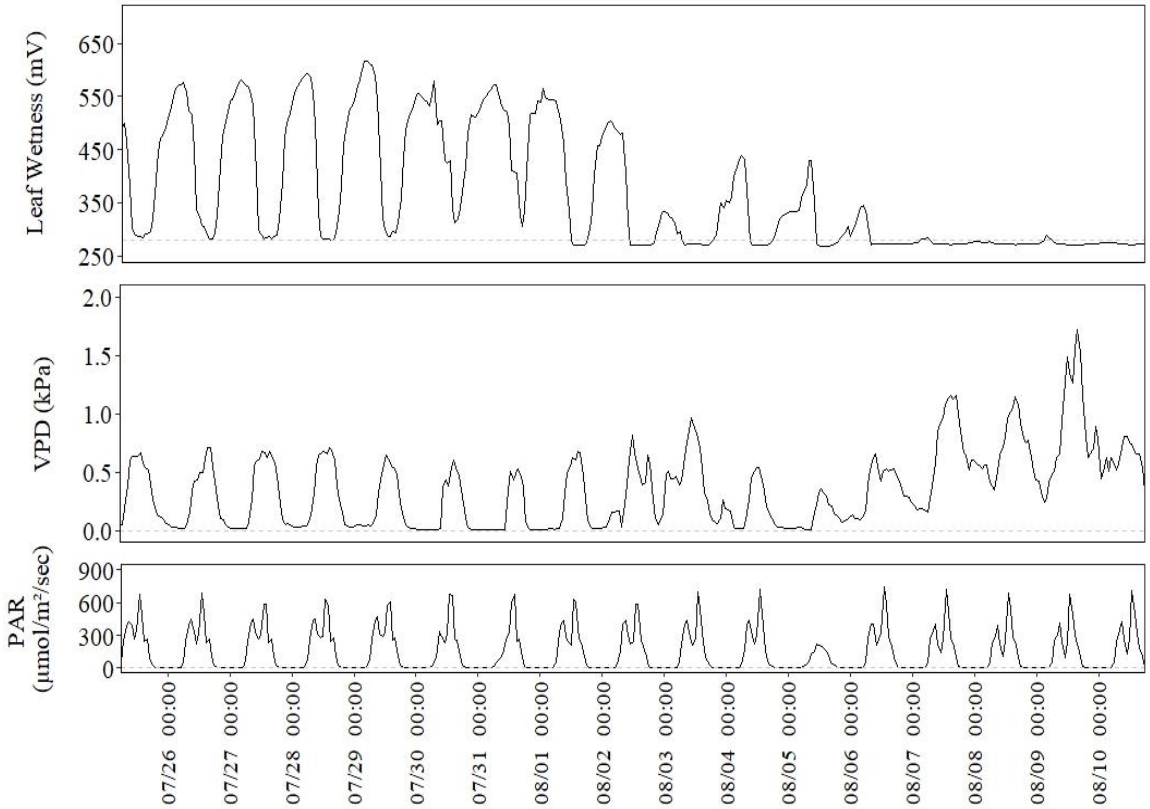

Figure 14: Diurnal trends in leaf wetness (top) and vapor pressure deficit (VPD, middle), and photosynthetically active radiation (PAR, bottom) for a period in late July / early August. A subset of data is presented to demonstrate climatic patterns when fog is present (Jul. 26 – Aug. 6) and absent (Aug. 7 – 10). Data are averages of four study sites.

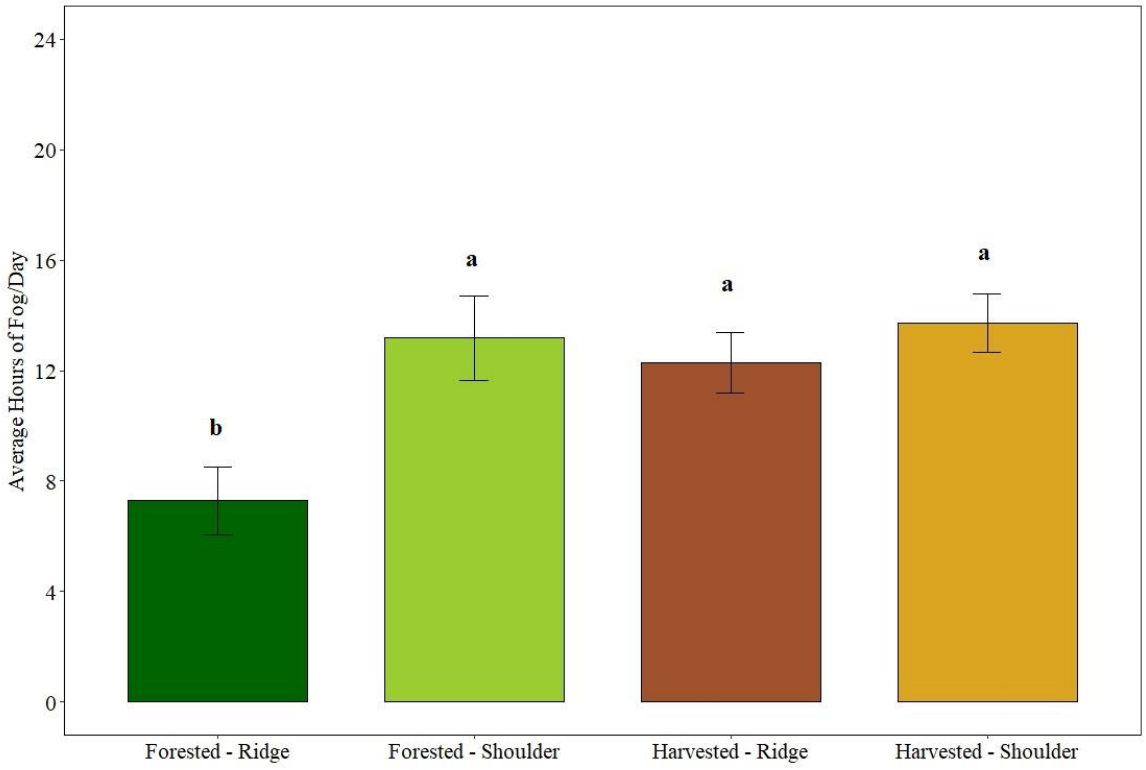

Figure 15: Seasonal average hours per day of fog presence at each site, as recorded by canopy leaf wetness sensors. Different letters indicate different means using Tukey's HSD test ($\alpha = 0.05$, df = 468). Error bars represent 95% confidence intervals.

5.3 Fog Deposition and Climatic Factors

During the 2020 fog season, winds came most frequently from the northwest at the forested sites, while the harvested sites had greater variability (Figure 16). The harvested shoulder site had a large portion of winds and fog deposition occur with northwesterly winds, but also with easterly winds. The harvested ridge had the greatest variation in wind directions, with the most frequent observations being from the north. High fog deposition (leaf wetness >750 mV) was generally associated with wind speeds between 0 and 2 m/s that primarily came from the northwest. Higher wind speeds (>3

m/s) were related to drier conditions (leaf wetness <350 mV). Lagged cross-correlation analysis between fog deposition and wind speed indicated a strong negative relationship, with the lowest wind speeds occurring simultaneously to the peak leaf wetness at most sites (Table 6; CI = 95%). Maximum VPD, mean air temperature, and maximum RH also had strong correlations to fog deposition, with no significant lag at any site. PAR had a strong, negative correlation with fog deposition at positive lags of 2-4 hours, indicating a decrease in solar radiation occurred after fog was already present on the landscape.

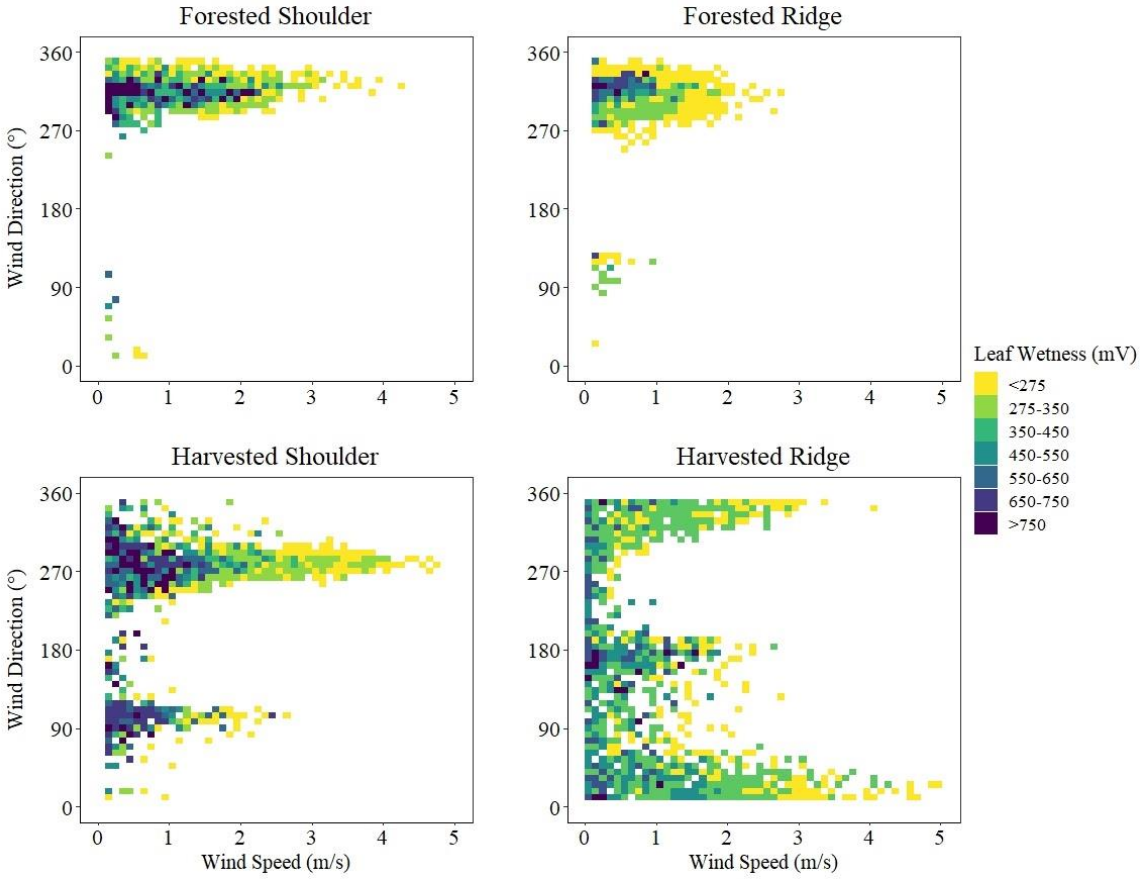

Figure 16: Relationship between mean wind speed (m/s), wind direction (°), and leaf wetness (mV) over the summer fog season. For display purposes, leaf wetness was binned into seven categories indicating the degree of moisture recorded by the LWS.

Table 6: Maximum significance correlation coefficients (MSC, 95% CI) and lag period between leaf wetness and meteorological variables. Variables include mean wind speed, maximum vapor pressure deficit (VPD), mean air temperature, maximum relative humidity (RH), and mean photosynthetically active radiation (PAR). Correlation and lag period were evaluated at hourly temporal resolution.

		Forested Shoulder	**Forested Ridge**	**Harvested Shoulder**	**Harvested Ridge**
Wind Speed (mean)	*MSC*	-0.873	-0.816	-0.824	-0.790
	Lag	0	0	1	0
VPD (max)	*MSC*	-0.876	-0.814	-0.941	-0.826
	Lag	1	1	0	0
Temperature (mean)	*MSC*	-0.909	-0.814	-0.964	-0.870
	Lag	1	1	0	0
RH (max)	*MSC*	0.880	0.751	0.940	0.797
	Lag	0	1	0	0
PAR (mean)	*MSC*	-0.556	-0.569	-0.831	-0.676
	Lag	2	4	2	3

5.4 Seasonal Trends in Soil Moisture

Soil moisture over the summer season varied with study site and sensor position. VWC of surficial soil (5 cm) at the harvested ridge site was zero at all three sensor positions: near the bole and drip edge of the study tree, as well as in a nearby opening (Figure 17a-c). Because these sensors reported positive VWC earlier in the year, observations of zero were assumed to indicate dry soils rather than sensor errors. At the bole position, shoulder sites in both the harvested and forested treatment groups

maintained the highest surficial soil VWC over the summer season (Figure 17a). At the drip-edge position, forested sites maintained the highest VWC over the season (Figure 17b). Both harvested treatment sites, on the other hand, reported near-zero soil VWC at 5 cm at the drip-edge for the majority of the season. Of the sensors positioned in the opening, only the forested shoulder site reported VWC values above zero across the entire season (Figure 17c). The remaining sites displayed a sharp decrease towards zero in early June and July. Surprisingly, in mid-August, the harvested shoulder site began recording positive (although noisy) VWC values at this position, lasting the remainder of the season with no clear trend.

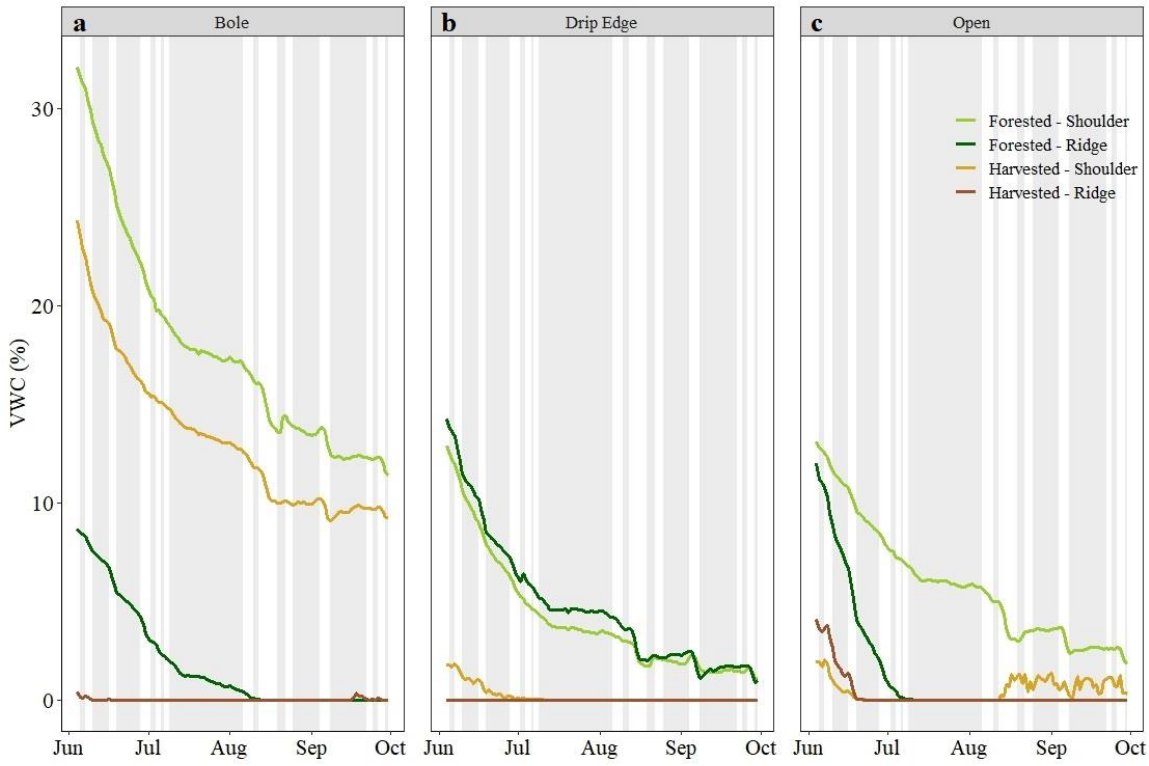

Figure 17: Mean daily volumetric soil water content (VWC, %) at 5 cm depth over the summer fog season (Jun. 04 – Sept. 30, 2020) by position- near the bole of the study tree (**a**), at the canopy drip edge (**b**), and in a nearby opening (**c**) at each study site. Background shading indicates days where average leaf wetness across sites reported fog presence (mV > 280).

Surficial soil (5 cm) VWC displayed a steep decline during the month of June (Figure 17a-c). As fog presence increased in July, the decline in VWC became more gradual and appeared to stabilize at sites that were reading positive values. Periods with no recorded fog in mid-August corresponded with sharp decreases in VWC at sites that were reading positive values.

Comparison of soil moisture at the 5 and 10 cm depths displayed the seasonal average VWC and variation both between and within study sites (Table 7). Similar to the

5 cm depth, the highest mean VWC of soil at 10 cm was at the bole position of the forested shoulder and harvested shoulder sites. Generally, VWC of soils at the 10 cm depth were higher than 5 cm at the bole position. At the drip-edge and opening positions, however, forested sites had lower VWC at 10 cm than at 5 cm. Comparing the mean VWC within each site based on sensor position, there were no clear trends at either the 5 or 10 cm depths.

Table 7: Mean daily VWC (%) and standard deviation (s) in parentheses of soils 5 and 10 cm below surface, organized by sensor position and study site.

		VWC (*s*), %		
Study Site	Soil Depth (cm)	Sensor Position		
		Bole	Drip Edge	Open
Forested Shoulder	5	17.7 (*4.7*)	3.9 (*2.6*)	5.8 (*2.6*)
	10	23.5 (*5.3*)	0.0 (*0.2*)	1.9 (*1.6*)
Forested Ridge	5	1.7 (*2.4*)	4.7 (*3.0*)	1.2 (*2.8*)
	10	8.7 (*3.6*)	3.5 (*1.9*)	0.6 (*1.4*)
Harvested Shoulder	5	13.2 (*3.5*)	0.2 (*0.4*)	0.4 (*0.9*)
	10	16.0 (*2.5*)	2.6 (*0.8*)	0.6 (*1.0*)
Harvested Ridge	5	0.0 (*0.1*)	0 (*0*)	0.3 (*0.8*)
	10	0.2 (*0.7*)	3.3 (*1.5*)	0.1 (*0.3*)

5.5 Soil Moisture Responses to Fog Events

Daily changes in mean VWC at 5 cm depth over the fog season were below 1% (Figure 18a-c). All sites and sensor positions reported decreases in daily VWC at the beginning of the season, some of which eventually reported no daily change due to flatlining at zero. Near the bole, increases generally occurred at the two shoulder sites, typically later in the season (i.e., Aug. and/or Sept.) and without any measurable precipitation. Of these increases, the forested shoulder site had the highest positive change occur in mid-August (Figure 18a). Both forested sites recorded increases in daily VWC, which also occurred later in the season and corresponded with a fog event (Figure 18b). Soil moisture at the harvested sites fell to zero at the drip edge position and did not record any changes for most of the summer fog season.

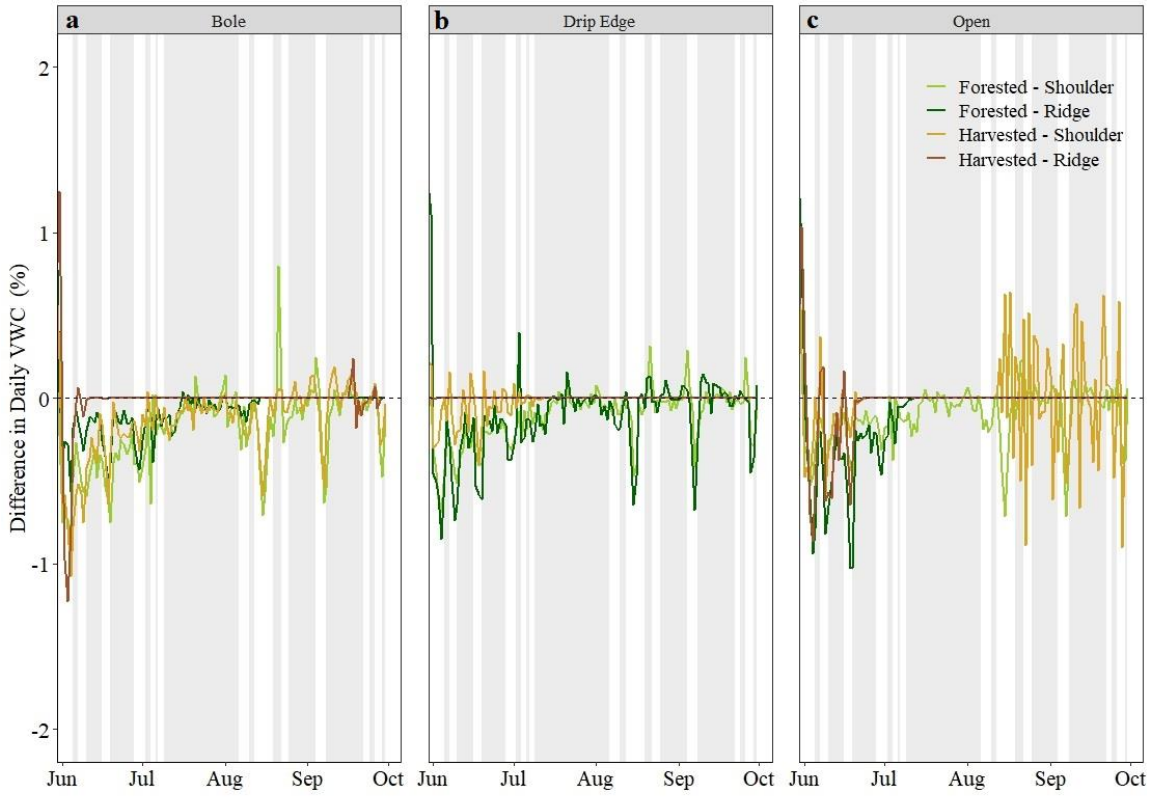

Figure 18: Difference in mean daily VWC (%) of soils 5 cm below the surface. Each graph represents sensor position at a study site: near the bole (**a**) and canopy drip edge (**b**) of a *S. sempervirens* tree, and in a nearby opening (**c**). Background shading indicates days where all sites were reporting fog presence, as determined by leaf wetness sensors. Graphs are centered around the horizontal zero line; increases from the previous day's soil moisture plot above the line, while decreases plot below the line.

Sensors located in an opening at each study site also recorded negative changes in VWC of soils (5 cm) at the beginning of the season (Figure 18c). The forested shoulder site was the only site at this position that recorded changes in daily VWC over the entire season. The remaining sites flatlined at zero for portions of the season, reporting no changes in daily VWC. Surprisingly, the harvested shoulder site began recording

increases in daily VWC in the opening around mid-August, which lasted the remainder of the season.

Deep soils (100 cm) displayed similar trends in moisture across sites as the surficial soils (5 cm). Soil moisture at 100 cm averaged across the bole and drip edge positions showed a slow, steady decrease over the summer fog season (Figure 19). Similar to surficial soils, the forested shoulder site had the highest soil moisture, recording VWC of 47% and 29% at the beginning and end of the season, respectively. The harvested shoulder site also had high VWC at the beginning of the season (45%) but decreased more rapidly and recorded 19% VWC at the end of season. Deep soil moisture at the ridge sites was generally lower than shoulder sites (Figure 19). Although the harvested shoulder site began the season with a higher VWC than the forested ridge site, they had nearly the same moisture at the end of the season (~20% VWC). Also similar to surficial soil moisture, the harvested ridge site had the lowest VWC of deep soils over the entire season.

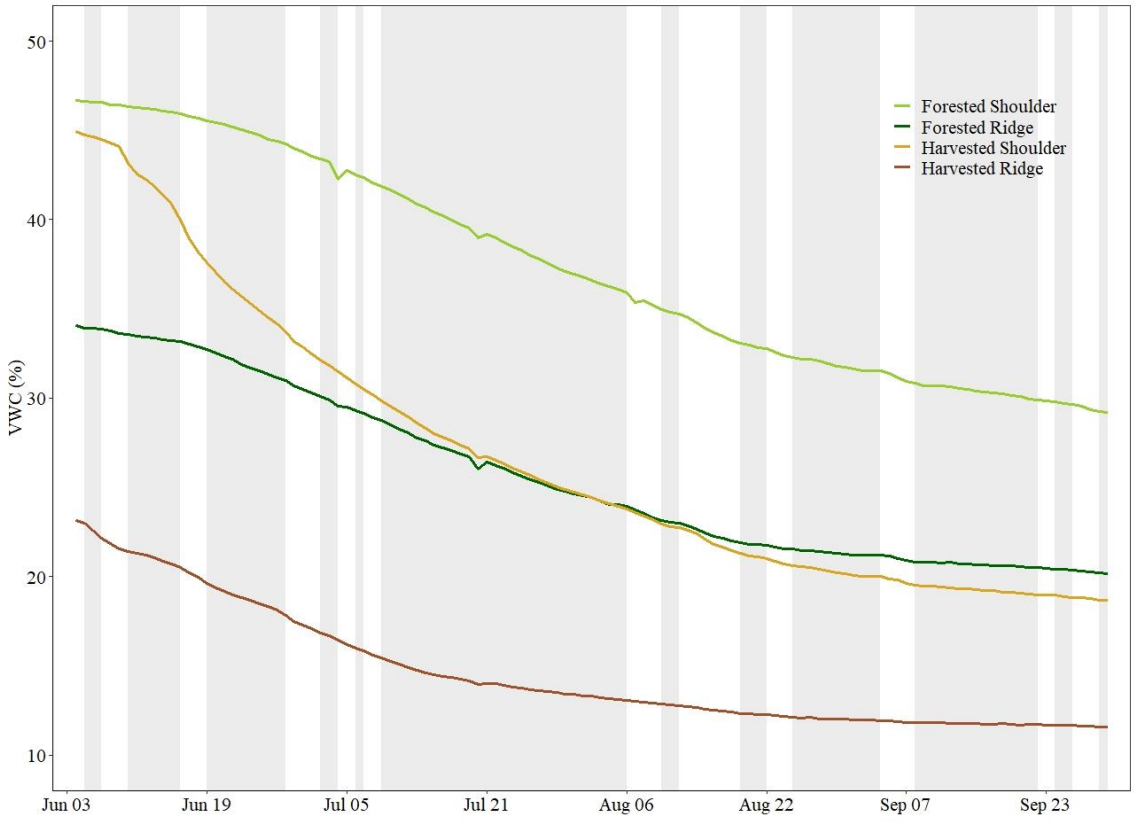

Figure 19: Mean daily volumetric water content (VWC, %) of soils at 100 cm depth over the summer fog season (Jun. 04 – Sept. 30). Study sites represented by colors and shaded background indicates fog presence. Values are averages of two soil moisture sensors, located near at the bole and at the drip edge of a *S. sempervirens* tree at each site.

5.6 Litter Moisture

Litter moisture following fog events varied among sites and over the 2020 summer season. The forested ridge site generally had consistently higher litter moisture than other study sites (Figure 20). However, this site did not display sharp increases in water content, but instead had slow increases following prolonged fog events. On the other hand, shoulder sites in both the forested and harvested treatments had sharp increases in daily litter moisture during several fog events over the season. Of these

increases, the mean daily voltage indicating the degree of wetness was generally higher at the forested shoulder site. Although the harvested shoulder site also displayed sharp increases, the mean daily voltage typically remained below the threshold that characterizes a "wet" sensor surface (280 mV). On September 15th, both harvested sites recorded sharp increases in litter wetness, while both forested sites had a minor increase. A rain gauge at the MET1 station reported a daily total of 0.23 mm on this day, which was below the study's threshold for a precipitation event (threshold = 1 mm/day). Interestingly, during the 1.09 mm precipitation event that occurred on September 24th, the harvested shoulder site had the highest response in litter wetness. The forested shoulder site also showed a minor increase to this precipitation event, but neither ridge site displayed notable responses (Figure 20).

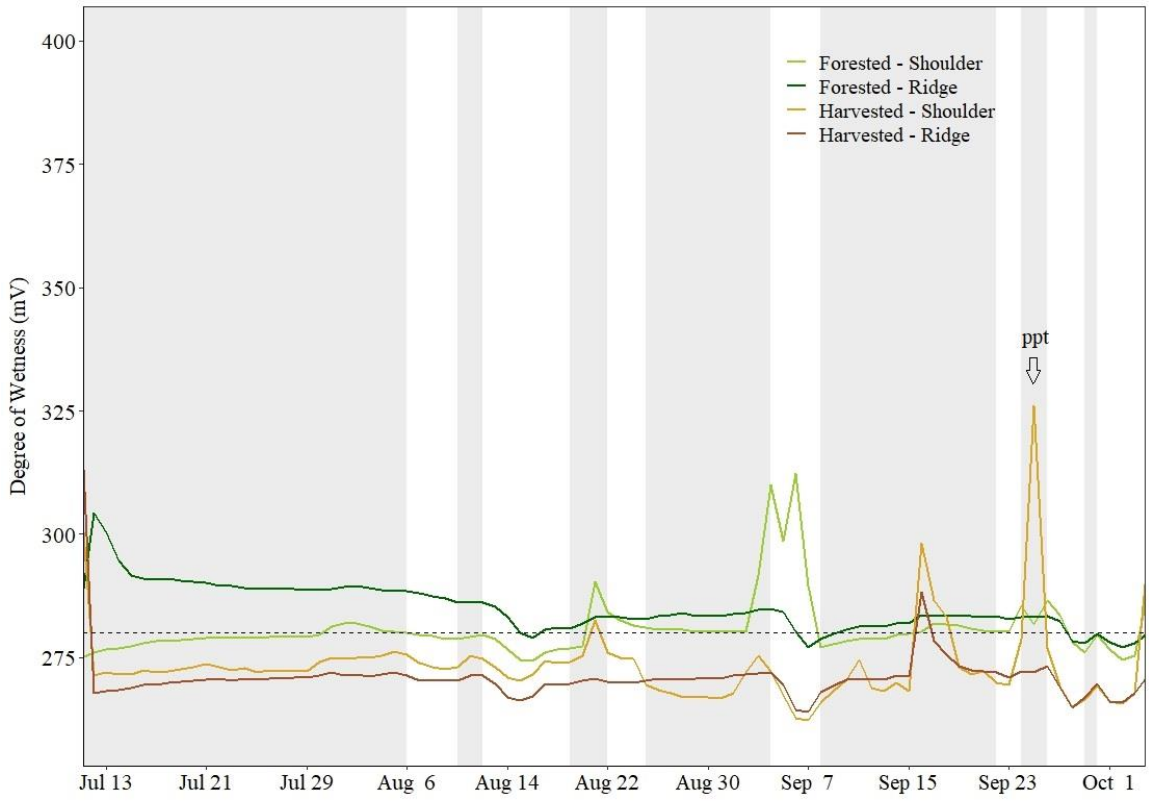

Figure 20: Litter wetness measured by leaf wetness sensor at each site, installed near the bole of a study tree. Dashed line at 280mV represents the threshold at which the sensor surface was considered saturated with water. A precipitation event (~1 mm) on September 24th is labeled as "ppt" on the figure. Background shading indicates days where all sites were reporting fog presence, as determined by canopy leaf wetness sensors.

The manual samples of litter moisture between mid-July and mid-August revealed that the forested shoulder site had the highest mean GWC (31.6%) and variability (s = 14.5%) over the sampling period (Table 8). When grouped by treatment, forested sites consistently reported higher mean litter GWC than harvested sites (Figure 21). The difference in litter moisture between treatment groups was highest in late July following a prolonged fog period (Figure 21). During a fog-free portion of August, the difference in

litter moisture between the two treatments decreased. The last litter sample, collected on August 21st, revealed considerable increases in litter moisture, with the highest magnitude observed at the forested shoulder site. A comparison of mean litter GWC using Welch's two sample t-test between all site combinations revealed that sites were statistically different from one another based on their treatment group rather than topographic position ($\alpha = 0.05$; Appendix C).

Table 8: Mean and standard deviation (s) of the Gravimetric Water Content (GWC, %) of the litter layer between mid-July and mid-August (n = 11).

Study Site	Mean	s
Forested - Shoulder	31.6	14.5
Forested - Ridge	29.9	5.49
Harvested - Shoulder	18.8	3.09
Harvested - Ridge	20.7	4.45

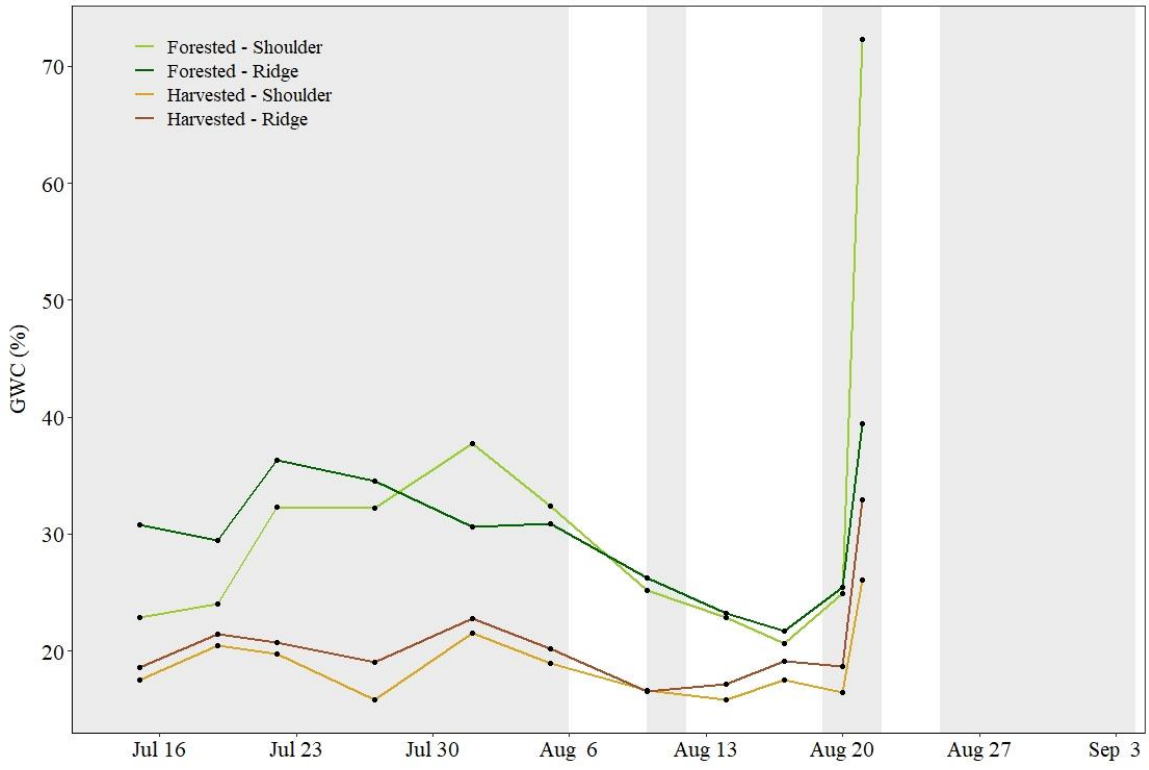

Figure 21: Gravimetric water content (GWC, %) of the litter at each study site during part of the summer season. Background shading indicates days where all sites were reporting fog presence, as determined by leaf wetness sensors.

5.7 Transpiration

A strong diurnal pattern in transpiration was evident at all study sites over the season, with the lowest sap flows occurring at night and early mornings (Figure 22). The forested ridge site had the smallest diurnal variation in transpiration, typically reaching similar daytime peaks as other sites but maintaining high transpiration rates at night, when all other study sites dropped. During these nightly drops in transpiration, most sites approached zero when fog was present, but the forested ridge site continued to have sap flow rates around 25% of the seasonal maximum. The harvested ridge and forested

shoulder sites frequently had transpiration rates below zero during foggy periods when VPD was at zero, indicating sap reversal and possible direct foliar uptake. The forested shoulder site consistently had lower daytime peaks than other sites during both fog presence and absence- reaching daily peaks around 50% of the maximum, compared to around 75% observed at the other sites.

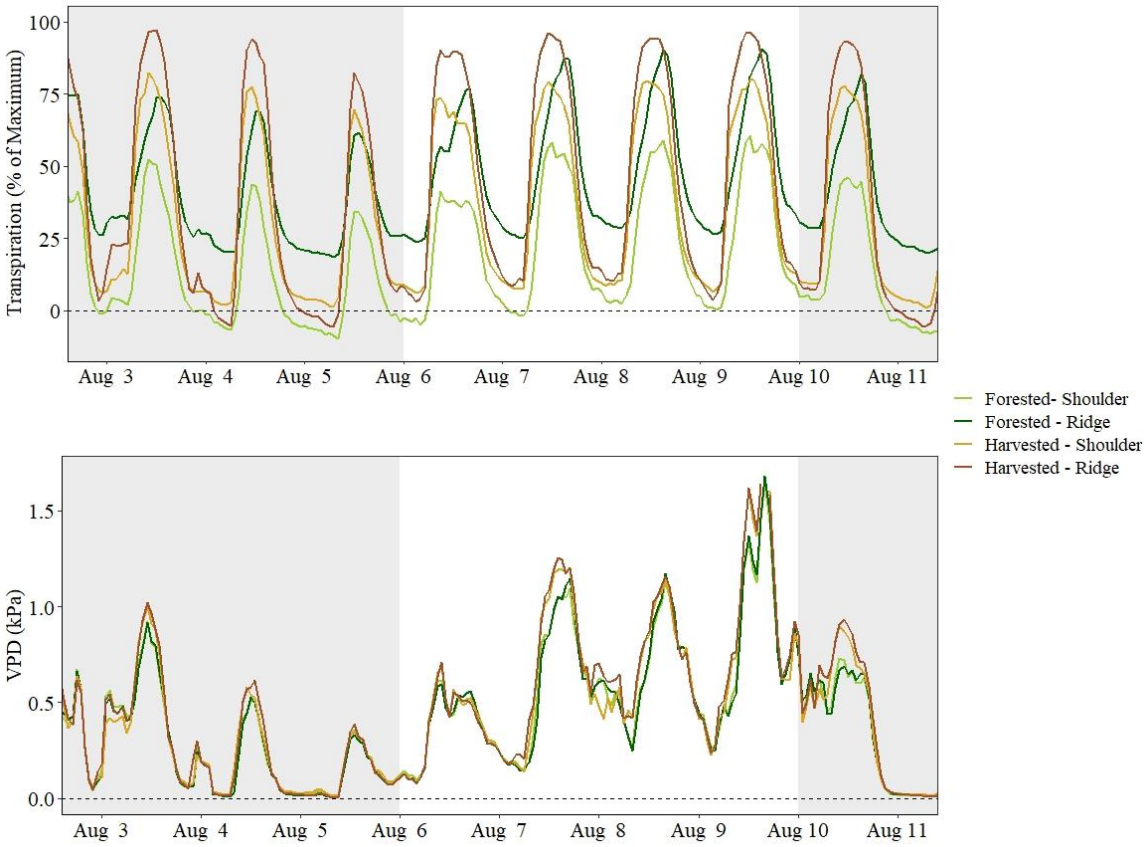

Figure 22: Typical diurnal trends in transpiration (top) and VPD (bottom) over periods with and without fog in August. Transpiration refers to sap flow velocity values displayed as percentage of site-specific seasonal maximum. VPD (kPa) is the hourly maximum at each site. Background shading indicates periods of leaf wetness at all sites. Dashed black line at zero is displayed to show when sap flow reverses and when VPD is zero. The subset of data presented here were chosen to display general patterns in transpiration and VPD during fog presence and absence.

Transpiration over the night-hours indicated varying degrees of responses when fog was present and absent. All sites had lower transpiration rates during foggy conditions (i.e., canopy LWS reporting wet sensor surface) than clear periods (Table 9). The change in mean nightly transpiration between the foggy and clear nights was twice as high at the harvested sites than the forested sites. The forested shoulder site had the lowest nightly transpiration rates during both foggy and clear nights. The forested ridge site, on the other hand, had the highest nightly transpiration rate during both foggy and clear nights and never fell below 17% of the maximum. Overall, the greatest variation in transpiration occurred on clear nights over the summer season, with harvested sites having the highest variation.

Table 9: Summary of nightly transpiration - including the mean, standard deviation (s), minimum, and maximum - over the summer season (Jun. - Sept.) when fog was present and absent. Transpiration refers to sap flow velocity expressed as percentage of site-specific seasonal maximum. Summary statistics were derived from hourly data.

Site	**Fog**	**Mean (s)**	**Minimum**	**Maximum**	**N (hours)**
Forested Shoulder	Present	-2.18 (8.03)	-11.87	44.62	634
	Absent	9.39 (13.51)	-8.44	79.30	412
Forested Ridge	Present	20.84 (2.36)	17.26	41.19	365
	Absent	31.63 (9.17)	20.00	73.48	683
Harvested Shoulder	Present	11.21 (15.81)	-0.45	80.88	849
	Absent	29.42 (23.37)	2.90	88.54	208
Harvested Ridge	Present	3.06 (13.42)	-7.88	70.35	599
	Absent	26.71 (24.54)	-1.07	89.48	438

All sites had occurrences of high nightly transpiration over the summer season, with some observations reaching 70-90% of the seasonal maximum on clear nights (Table 9). On foggy nights, the maximum observed transpiration at forested sites dropped to ~ 40% of the seasonal maximum. Maximum nightly transpiration at the harvested sites, on the other hand, was still 70-80% of the seasonal maxima. This was only slightly lower than the maximum transpiration on clear nights at these sites. Meanwhile, minimum observed transpiration was negative at both the forested shoulder and harvested ridge sites, regardless of foggy versus clear nights (Table 9). Overall, the forested shoulder site spent approximately 55% of the summer night hours with negative sap flows, which was greater than all other sites (Table 10). The harvested ridge site had the second-greatest amount of reverse sap flows at ~36% of the summer nights hours, while the harvested shoulder site reported only 1%. The forested ridge site did not have any occurrence of reverse sap flow over the 2020 summer season.

Table 10: Percentage of summer night hours with reverse sap flow at each study site. Reverse sap flow was defined as the sap flow velocity being less than zero.

Site	**Time with Reverse Sap Flow (%)**
Forested - Shoulder	55
Forested - Ridge	0
Harvested - Shoulder	1
Harvested - Ridge	36

Daily trends in transpiration over the summer season showed that all sites displayed a clear increase in transpiration when fog was no longer present (Figure 23). Early in the summer season, transpiration rates appeared relatively similar across all sites. As fog presence increased over the month of July, the forested shoulder site began

deviating from other sites by recording lower transpiration rates that lasted the remainder of the season (Figure 23). The difference in transpiration between this site and the others increased during prolonged periods of fog (late July – early Aug.) and became smaller during fog-free periods (mid-Aug.). Over the season, as transpiration rates continued to decrease during fog presence at the forested shoulder site, occurrences of negative mean daily transpiration occurred at this site but not at any others.

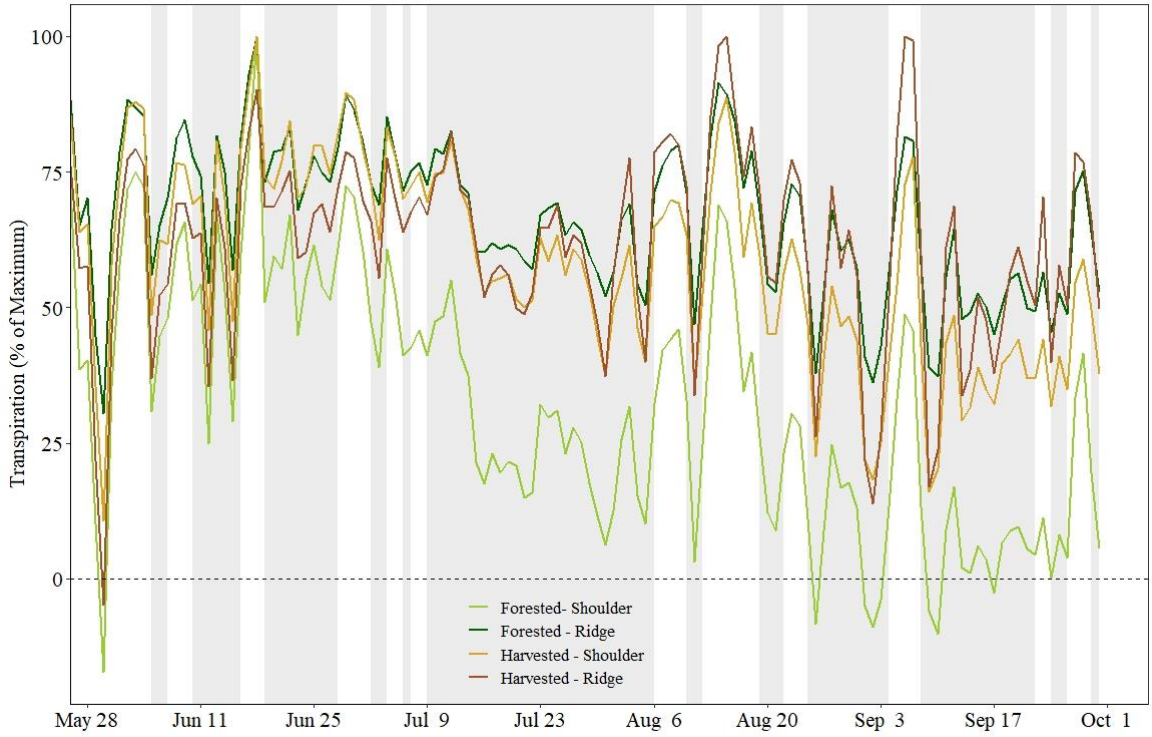

Figure 23: Mean daily transpiration of one *S. sempervirens* tree at each study site over the summer fog season. Sap flow velocity expressed as percentage of site-specific seasonal maximum. Background shading represents periods when fog was present at all sites, but the record runs from Jun 04 until Sept. 30.

A seasonal summary of daily transpiration rates at each site supported the observation of the forested shoulder site deviating from other sites (Table 11). The seasonal mean transpiration at the forested shoulder site was ~ 32% of the seasonal

maximum, while the remainder of sites averaged around 60% of their respective maximums. Tukey's HSD results indicated that mean seasonal transpiration at the forested shoulder site was different from all others. This test also revealed that mean transpiration rates at the harvested ridge site were not significantly different from the rates at the harvested shoulder or the forested ridge sites.

Table 11: Summary of daily transpiration including the mean and standard deviation (s) at each study site over the summer fog season (June – Sept.). Transpiration refers to sap flow velocity expressed as percentage of site-specific seasonal maximum. Results of Tukey's HSD are also presented, with a shared letter indicating no statistical difference in the means ($\alpha = 0.05$).

Site	**Mean (s)**	**Tukey HSD Group**
Forested - Shoulder	32.24 (23.33)	c
Forested - Ridge	66.73 (13.64)	a
Harvested - Shoulder	58.80 (18.27)	b
Harvested - Ridge	62.42 (16.86)	ab

Kendall tau-b correlation coefficients indicated the strength and direction of relationships between transpiration and climatic variables at each study site. Although all sites were evaluated individually, correlation coefficients were generally on a similar order of magnitude for each climatic variable across sites (Table 12; all p-values < 2.2e-16). VPD had the strongest correlation with transpiration at each study site, ranging from positive 0.592 to 0.634. Following VPD, PAR was also positively correlated with transpiration at all sites. Wind speed had a relatively strong positive correlation at the forested ridge site (0.445), followed by the forested shoulder and harvested shoulder sites

(0.385 and 0.361, respectively). Transpiration at the harvested ridge site, however, had the lowest correlation value with wind speed with a correlation coefficient of 0.183. Leaf wetness surprisingly had a relatively strong negative correlation with transpiration at both harvested sites (coefficients of approximately -0.55), and a slightly weaker one at the forested sites (coefficients of approximately -0.38).

Table 12: Kendall tau-b correlation coefficients between hourly sap flow velocity (represented as % of seasonal maximum) and climatic variables (VPD, PAR, wind speed, and leaf wetness). Each of the following correlation coefficients generated by the Kendall tau-b test had a p-value of < 2.2e-16.

Site	**VPD**	**PAR**	**Wind Speed**	**Leaf Wetness**
Forested - Shoulder	0.615	0.507	0.385	-0.399
Forested - Ridge	0.634	0.546	0.445	-0.365
Harvested - Shoulder	0.592	0.520	0.361	-0.525
Harvested - Ridge	0.604	0.534	0.183	-0.581

6. DISCUSSION

6.1 Fog at the Caspar Creek Experimental Watersheds

Observations of visibility, leaf wetness, and soil moisture monitored fog presence at the Caspar Creek Experimental Watersheds (CCEW) over the 2020 summer season. The month of July had the greatest seasonal fog presence, while the highest increases in soil and litter moisture occurred in August and September. Fog presence generally followed a diurnal pattern—leaf wetness observations indicated fog rolled onto the landscape in the evening, typically several hours before solar radiation reached its

minimum (Table 6). Temperature decreased and relative humidity increased during fog presence, which caused a decrease or full elimination of the VPD, with cascading decreases in sap flow. Observations of wind and leaf wetness indicated that the highest fog deposition occurred at low wind speeds, generally coming from the northwest direction (Figure 16).

Fog development depends on several conditions related to the strength of the Pacific High, sea surface temperatures, and atmospheric pressure gradients. The Pacific High is typically the strongest during the summer and a strong temperature gradient develops between the ocean and land as the land heats and cools. Although temperatures are relatively stable along the coast, rising inland temperatures over the summer months strengthen this pressure gradient, causing advection of fog onto the landscape. Advective fog is most often observed beginning in late July and lasting through late September at the CCEW study sites. Satellite-derived observations from 1996 – 2014 along the California coast demonstrated a pattern of a northward migration in coastal low cloud cover, which includes fog and stratus clouds. Low clouds along the coast of northern California are most prevalent in July, generally peaking in late July/early August at the northernmost extent (Clemesha et al., 2016). This is supported by other studies which indicate the highest fog presence occurs in August in northern California (Santiago and Dawson, 2014), as well as local anecdotes that refer to the month of August as "fog-gust". Land insolation and heat capacities of the ocean and land drive the diurnal cycle of fog, causing fog advection onto the landscape in the evenings and dissipation in the morning. This diurnal trend in fog presence was observed at the CCEW and supports the

observations of other studies in coastal California (Fischer and Still, 2007; Hiatt et al., 2012; Rastogi et al., 2016).

Over the 2020 fog season, the highest leaf wetness observations at the CCEW generally occurred at relatively low wind speeds from the northwest with< 2 m/s. As advective winds transport fog across the landscape, high wind speeds may cause turbulence that leads to the dissipation of fog layers (Dawson, 1998). However, some studies contradict this relationship and suggest higher wind speeds generate more contact between fog particles and condensation surfaces (Hiatt et al., 2012; Pryet et al., 2012), resulting in greater fog deposition. Fog deposition on Santa Cruz Island, California was found to occur primarily at northwest winds between 2-3 m/s (Fischer and Still, 2007), and prevailing summer winds in northern California are typically from the northwest directions. Based on the orientation of the CCEW study sites in relation to the origin of fog (i.e., Pacific Ocean), the highest deposition was also expected to occur with northwesterly winds. This is typically found in other studies along the California coast, which found the highest rates of fog deposition with north/northwesterly winds (Johnstone and Dawson, 2010; Hiatt et al., 2012).

6.2 Contribution of Fog Drip to Forest Floor

6.2.1 Soil and Litter Moisture

Over the 2020 summer fog season, evidence of fog deposition was found at both treatments. Surficial soil VWC increased following fog events, even in an opening. Daily increases in surficial (5 cm) soil moisture following fog were less than 1% VWC across the four study sites. However, VWC observations over the entire season indicated that

fog presence noticeably reduced soil drying (Figure 17). Overall, surficial soils were wettest near the boles of *S. sempervirens* trees at the two shoulder sites, which also reported the highest intensities of leaf wetness. Similarly, litter water content using both the litter LWS and gravimetric samples increased following fog events. Forested sites had a higher overall litter water content than harvested sites, although the difference between the two decreased during fog-free periods as the forested sites dried (Figure 21).

Climatic observations at each study site indicated that fog events reduced and/or eliminated VPD. Thus, the reduced drying rate of surficial soils during fog events was likely due to reduced evaporative losses. Rather than volumetric inputs, the reduction of VPD by fog is considered to be a great ecohydrological benefit during periods of drought in both California (Burgess and Dawson, 2004; Fischer et al., 2009; Carbone et al., 2011) and other global fog-inundated ecosystems (Hildebrandt et al., 2007; Ritter et al., 2008). For example, in a coastal pine ecosystem on Santa Cruz Island, lower rates of evaporation from soil surfaces during fog events was the largest factor in relieving plant and microbial water stress (Carbone et al., 2013). At the CCEW, lower evaporative losses associated with fog presence and canopy cover may be responsible for the differences in litter moisture between the treatments. Although sites in both treatments recorded increased litter moisture following fog events, forested sites had higher litter GWC than harvested sites over the entire season. Daytime evaporative losses at the harvested sites on clear days likely drove the site differences, as harvested sites had higher exposure to direct solar radiation than the forested sites. Therefore, the combination of forest cover and fog presence were responsible for higher soil and litter moisture levels at the forested sites.

Small daily increases in surficial soil moisture following fog events were observed at all sensor positions, including in canopy openings. Shoulder sites in both the forested and harvested treatments reported increases in soil moisture in the opening. This was especially surprising at the harvested shoulder site opening, which recorded zero VWC over most of the season, until a short fog event in August caused positive VWC readings (Figure 17c). Although this fog event was followed by one of the hottest days of the season, this sensor continued reading positive VWC for the remainder of the season. Fog that was travelling close to the ground surface and accumulating on litter and woody debris may have driven the deposition of fog water in openings; this fog water may have eventually percolated down to the mineral soil. Higher wind speeds may also cause fog deposition in canopy openings; small fog water droplets may aggregate to larger sizes during high winds, creating a drizzle-type precipitation (Torregrosa et al., 2020). Previous studies of fog drip at the CCEW indicated that clearings receive similar amounts of fog drip as full-canopy sites (Keppeler, 2007). Generally, studies of fog drip have found that soils in clearings are significantly drier than under canopies (Ataroff and Rada, 2000; Fischer et al., 2009). However, studies have found that although fog deposition may be smaller in clearings than under full canopies, collectors in clearings nevertheless accumulate water in fog-inundated forests of the Pacific Northwest (Harr, 1982; Ingwersen, 1985; Ewing et al., 2009), including ones dominated by *S. sempervirens* (Dawson, 1998).

6.2.2 Interception of Fog Drip

Although surficial soil and litter moisture increased following fog events at all study sites, these increases were relatively low in magnitude. Interception loss by foliage

and bark surfaces may be responsible for the low quantities of fog drip reaching the forest floor. Given the high surface area of needles and absorbent bark of *S. sempervirens*, accumulated fog water may be stored and either evaporated back into the atmosphere or directly absorbed by the tree. Studies of interception loss at the CCEW revealed that approximately 22% of annual precipitation is stored on canopy surfaces and evaporates before reaching the forest floor (Reid and Lewis, 2009). The interception of fog drip by vegetation was also significant in a Venezuelan cloud forest, which reported foliage intercepted approximately 51% of incoming water (Ataroff and Rada, 2000). Interception by bark may also be significant in the coast redwood forest. The bark of both dominant tree species (*S. sempervirens*, *P. menziesii*) can store significant amounts of water, with storage capacities unlikely exceeded during most precipitation or fog events. Bark samples taken at the CCEW indicate that *S. sempervirens* can absorb up to 0.45 cm^3 of water for every cm^3 of bark, and *P. menziesii* up to 0.15 cm^3 of water per cm^3 of bark (Reid and Lewis, 2009).

Besides evaporation, fog water deposited on foliage and bark can be directly absorbed and used in transpiration, refilling of desiccated tissues, or transported to roots (Burgess and Dawson, 2004; Earles et al., 2015). Direct foliar uptake, although minimal in terms of daily water use, can occur in most of the dominant overstory and understory species of the coast redwood forest (Dawson, 1998; Burgess and Dawson, 2004; Limm et al., 2009). One study on bark absorption revealed that *S. sempervirens* bark could absorb biologically significant amounts of water during prolonged wetting events, such as fog (Earles et al., 2015). Finally, in the event that fog deposition does produce drip that begins falling to the ground, it is possible that understory foliage intercepts the water

before it reaches the litter layer or mineral soil. A survey of understory vegetation at each study site indicated that both the forested and harvested treatments have significant densities of vegetation below the overstory (Table 13).

Table 13: Percentage (%) of canopy cover by vegetation height class at the four study sites.

Study Site	**Canopy Cover (%)**			
Vertical Height (m)	*0 – 0.6 m*	*0.6 – 1.8 m*	*1.8 – 4.9 m*	*> 4.9 m*
Forested - Shoulder	15	20	40	75
Forested - Ridge	20	40	50	80
Harvested - Shoulder	40	35	15	20
Harvested - Ridge	70	65	15	10

6.3 Influence of Fog on Overstory Transpiration

Transpiration rates, reflected by sap flow velocity, had a strong diurnal pattern and displayed responses to fog presence. Over the 2020 fog season, most sites maintained relatively high transpiration rates through the night, averaging near 30% of the summer maximum on clear nights. Fog presence reduced nightly transpiration rates; the greatest difference in mean nightly transpiration between clear and foggy nights was at the harvested sites (Table 9). The forested shoulder site was anomalous, reporting lower transpiration rates than other sites during both clear and foggy nights. This site also had the greatest amount of reverse sap flow—55% of the total nighttime hours—and suggests direct uptake of fog water (Table 10). The overall seasonal trend indicated that the forested shoulder site benefitted the most from fog. Following foggy periods, mean daily transpiration at the forested shoulder site was lower than the other sites (Figure 23).

The harvested ridge site had high daily transpiration rates over the entire season, despite having the lowest soil moisture. Following the soil-plant-atmosphere continuum model describing water transport during transpiration, available subsurface water is necessary for transpiration to occur. Of our study sites, the harvested ridge site had the lowest surficial (5 cm) and deep (100 cm) soil moisture but maintained the highest peaks in daily transpiration late into the summer season. With minimal precipitation during the observed period, the observed high rates of transpiration may be supported by fog presence. The harvested ridge site had the second-highest occurrence of reverse sap flow, with approximately 36% of nightly observations recording direct uptake of fog water (Table 10). This supports findings by Simonin et al. (2009), which demonstrated the absorption of fog water decoupled *S. sempervirens* dependence on soil water resources. Bark uptake of water during multi-day wetting events has also been found in *S. sempervirens*, which may facilitate relatively constant transpiration and growth over the summer fog season (Earles et al., 2015).

Although the forested shoulder site had the highest rate of reverse sap flow and the highest soil water content, transpiration rates were the lowest during both foggy and clear nights, as well as over the entire season. This may have been caused by excessive deposition of fog water on foliage, which can suppress transpiration and thereby decrease photosynthesis and reduce growth. Indeed, the forested shoulder site frequently had leaf wetness intensities higher than other sites (Figure 13). Direct foliar uptake of fog typically comprises a small portion of the daily water used by *S. sempervirens* (Burgess and Dawson, 2004) and no increases in soil moisture following this absorption have been observed in other studies. However, one study of direct foliar uptake in a Brazilian cloud

forest revealed that fog directly absorbed by leaves was transported to plant roots and showed up in soil rhizosphere of *Drimys brasiliensis* Miers. (Winteraceae), a common woody species in that ecosystem (Eller et al., 2013). It is possible that foliar uptake of fog water generated the higher soil water content at the forested shoulder site. However, our observations were based on one *S. sempervirens* tree, and other site-specific characteristics may drive the soil moisture dynamics at this site. Therefore, a more thorough study is required to investigate the relationship between transpiration, direct foliar uptake, and soil moisture, particularly since the harvested shoulder site had similar leaf wetness rates to the forested shoulder site yet continued to have high transpiration rates.

Magnitudes of sap flow reversal and nightly transpiration observed at the CCEW sites were both slightly higher than found by other studies of *S. sempervirens* trees. These were slightly higher than the findings by Burgess and Dawson (2004), which found instantaneous reverse flow rates between 5-7% of the maximum transpiration. These values between the two studies are on similar orders of magnitude, despite differences in location, year, and size of the *S. sempervirens* trees observed. Their study also found nightly transpiration rates exceed 20% of maximum transpiration, with the highest transpiration rates being around 40% of the maximum on dry nights (Burgess and Dawson, 2004). During the 2020 fog season, our study sites typically averaged nightly transpiration rates up to 30% of the maximum transpiration on clear nights, but occasionally reached rates between 70 - 90% of the transpiration maximum. This rate of water loss was reduced during foggy nights in our study, with the greatest difference in transpiration between clear and foggy nights occurring at both harvested sites (Table 9).

6.4 Variation in Fog Deposition, Soil Moisture, and Ecosystem Responses

Although evidence of fog deposition and transpiration reduction was present at all sites over the 2020 fog season, responses varied in timing and magnitude across the four study sites. Leaf wetness measurements following most fog events were higher at sites located at the hillslope shoulder (Figure 13). Rather than solely an influence of topographic position, this was most likely reflecting variation in site-specific characteristics. The elevation difference between shoulder and ridge sites was relatively small (22 m) and although there was no available data on local heights of the fog layer, fog banks tend to be several hundred meters thick, with topography between 200 – 400 m typically receiving the most fog along the California coast (Fischer et al., 2009). Elevation of our study sites fit into this range, although fog was also observed at lower elevations (approximately 25 m) in the towns of Fort Bragg and Caspar, which are both closer to the coast than our field sites. Thus, because of the small differences in elevation, other factors must be influencing the disproportionately greater fog deposition that is occurring at the shoulder sites in our study.

6.4.1 Topographic Influences

Both shoulder sites had a northerly aspect (351 – 357°) compared to the two ridge sites, which had more westerly aspects (288 – 294°). Prevailing summer winds in the region that carry fog across the landscape come from the north/northwest direction, as found by our observations and other studies (Figure 16; Torregrosa et al., 2016). Although the harvested shoulder site reported fog deposition associated with northwest and easterly wind directions, the forested shoulder site received most winds from the northwest (Figure 16). Therefore, based on their aspect and prevailing winds, shoulder

sites may have a direct delivery of fog-rich winds compared to the ridge sites. Analysis of fog and low clouds (FLCC) along the northern California coast revealed that local terrain orientation is an important factor in determining the amount of fog received by a region. Terrain oriented to face the prevailing northwest winds had the greatest amount of FLCC cover, including the Mendocino Coast (Torregrosa et al., 2016).

6.4.2 Species Composition

Species composition varied slightly across sites, which could also explain variation in fog deposition and soil moisture. Majority of the overstory consisted of *S. sempervirens* trees except the forested shoulder site, which has a greater proportion of *P. menziesii* (Table 2). Field observations over the 2020 fog season and previous years (Keppeler, E.T., personal communication, 3/16/2021) indicated significant fog drip occurring under *P. menziesii*, sometimes leaving puddles along roads (Figure 24). This was not typically observed under *S. sempervirens* canopies. The higher proportion of *P. menziesii* at the forested shoulder site may be responsible for the higher rates of fog deposition recorded by leaf wetness and soil moisture sensors.

Figure 24: Fog drip causing puddles on the road, under the canopy of *P. menziesii*. Photograph taken August 21, 2020.

No known studies have directly compared the volumes of fog drip produced by *S. sempervirens* and *P. menziesii* in the coast redwood forest. However, observations taken from varying studies of fog drip support field observations of higher volumes of drip produced by *P. menziesii* than *S. sempervirens*. One study on the San Francisco Peninsula found a seasonal total of fog drip to be around 56 mm under a *S. sempervirens* canopy (Oberlander, 1956). In another study, in the Bull Run Watershed in Oregon, a seasonal

total under a *P. menziesii* canopy was approximately 425 mm over a summer fog season (Azevedo and Morgan, 1974). Although these two studies were conducted in separate regions, they have a similar Mediterranean climate dominated by summertime fog. Needle physiology may explain the difference between the two species; observations of needle structure provide insight into the possible fate of deposited fog water (Figure 25). Leaf area indices (LAI) of *S. sempervirens* are among the highest in the world (Westman and Whittaker, 1975; Pelt et al., 2016) and their needles are spaced closely together, with a feather-like appearance that may allow for prolonged storage of deposited water (Figure 25a). The needles of *P. menziesii*, on the other hand, have more spacing between individual needles, creating gaps for fog water droplets to fall through (Figure 25b). Although *P. menziesii* has demonstrated a slightly higher rate of direct foliar uptake than *S. sempervirens* (Limm et al., 2009), the high surface area of *S. sempervirens* needles may allow more storage and evaporation of deposited water back into the atmosphere. The absorption capacity of bark also varies between the two species - *S. sempervirens* bark can store higher volumes of water than *P. menziesii* bark (0.45 and 0.15 cm^3/cm^3, respectively; Reid and Lewis, 2009). Therefore, it is possible that the forested shoulder site had higher fog deposition than other sites because it was dominated by *P. menziesii* rather than *S. sempervirens*, but further investigation of fog drip between the two species is needed.

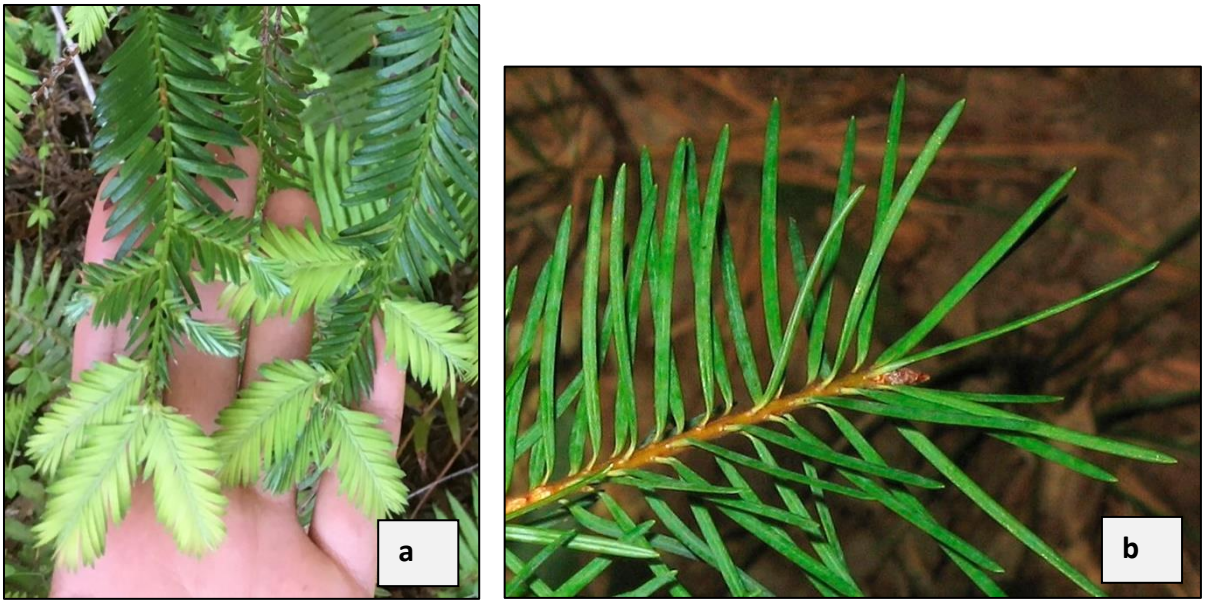

Figure 25: Needle comparison of *S. sempervirens* (a), *P. menziesii* (b)

The density and species composition of understory vegetation may also influence the amount of fog drip that reaches litter and surficial soils. Understory plant density surveys indicated that ridge sites in both treatments had higher plant densities within 0-0.6 m and 0.6-1.8 m of the ground than shoulder sites (Table 13). The higher densities of understory plants at the ridge sites may have intercepted fog drip before it reached the forest floor. Limm et al. (2009) indicated that many understory species of the coast redwood forest are also capable of direct foliar uptake of fog, with western sword fern (*Polystichum munitum*) exhibiting the highest uptake rates. However, a 2019 study investigating understory vegetation at the CCEW revealed that the harvested and forested watersheds did not have significant differences in understory density, species richness, or diversity (Hammerschmidt et al., In Review). The forested watershed, however, had greater development of a mid-story, consisting of mature *Vaccinium ovatum* (evergreen huckleberry), *Notholithocarpus densiflorus* (tan oak), and *Rhododendron macrophyllum*

(Pacific rhododendron). Interestingly, that study also found that both understory transpiration rates and soil moisture (within the upper 20 cm) were higher at the harvested watershed than the forested watershed. The discrepancy in findings between the studies may be the result of different sampling years, sampling methods, and sites included in the study. Our study only focused on the two uppermost sites of the hillslope in each watershed, whereas all five sites along the topographic gradient were included in the analysis conducted by Hammerschmidt et al. (In Review). Overall, it is difficult to conclude the effects of treatment, fog deposition, and soil moisture due to the small sample size included in this study (n = 4). However, these results display the importance of further studies of fog drip, soil moisture, and transpiration rates of both the overstory and understory at the Caspar Creek Experimental Watersheds.

7. CONCLUSION

The presence of fog provides ecohydrological benefits to ecosystems around the world primarily by relieving water stress during periods of drought. Fog dynamics were characterized at the Caspar Creek Experimental Watersheds and compared between two topographic positions and two timber harvest treatments. Fog drip inputs to surficial soils and litter layers were observed at all sites but were relatively small in magnitude. Fog reduced transpiration rates of *S. sempervirens* trees in both harvest treatments, but the greatest difference in transpiration between clear and foggy nights occurred at the harvested sites. Reverse sap flow was also observed during fog events, indicating direct foliar uptake, which may have sustained high transpiration rates at the harvested ridge site over the summer season. Variation in fog deposition was observed at all sites and

may be driven by site-specific characteristics such as hillslope aspect and species composition, with some observations indicating higher fog drip occurred under *P. menziesii* rather than *S. sempervirens*.

This study contributes to understanding fog dynamics in the coast redwood forest. With most studies examining forests consisting of old-growth *S. sempervirens*, our study examined fog dynamics in a managed third-growth forest. Observations of leaf wetness, soil moisture, and sap flow indicated the presence and ecosystem responses to fog over the 2020 summer drought season. Overall, there were no evident effects of timber harvest on fog deposition. Nevertheless, our results demonstrate the need to continue investigating fog dynamics at the Caspar Creek Experimental Watersheds, including the variation in fog deposition beneath *S. sempervirens* and *P. menziesii* canopies.

REFERENCES

American Meteorological Society. (2012). Fog. Glossary of Meteorology. Retrieved January 2020, from http://glossary.ametsoc.org/wiki/Fog

American Meteorological Society. (2012). Radiation Fog. Glossary of Meteorology. Retrieved January 2020, from http://glossary.ametsoc.org/wiki/Radiation_fog

American Meteorological Society. (2012). Upslope Fog. Glossary of Meteorology. Retrieved January 2020, from http://glossary.ametsoc.org/wiki/Upslope_fog

Ataroff, M., & Rada, F. (2000). Deforestation impact on water dynamics in a Venezuelan Andean cloud forest. *Ambio*, *29*(7), 440–444. https://doi.org/10.1579/0044-7447-29.7.440

Azevedo, J., & Morgan, D. L. (1974). Fog Precipitation in Coastal California Forests. *Ecology*, *55*(5), 1135–1141.

Baguskas, S. A., Peterson, S. H., Bookhagen, B., & Still, C. J. (2014). Evaluating spatial patterns of drought-induced tree mortality in a coastal California pine forest. *Forest Ecology and Management*, *315*, 43-53.

Barbosa, O., Marquet, P. A., Bacigalupe, L. D., Christie, D. A., Del-Val, E., Gutierrez, A. G., … Armesto, J. J. (2010). Interactions among patch area, forest structure and water fluxes in a fog-inundated forest ecosystem in semi-arid Chile. *Functional Ecology*, *24*(4), 909–917. https://doi.org/10.1111/j.1365-2435.2010.01697.x

Burgess, S. S., Adams, M. A., & Bleby, T. M. (2000). Measurement of sap flow in roots of woody plants: a commentary. *Tree Physiology*, *20*(13), 909-913.

Burgess, S. S., Adams, M. A., Turner, N. C., Beverly, C. R., Ong, C. K., Khan, A. A., & Bleby, T. M. (2001). An improved heat pulse method to measure low and reverse rates of sap flow in woody plants. *Tree physiology*, *21*(9), 589-598.

Burgess, S. S. O., & Dawson, T. E. (2004). The contribution of fog to the water relations of Sequoia sempervirens (D. Don): Foliar uptake and prevention of dehydration. *Plant, Cell and Environment*, *27*(8), 1023–1034. https://doi.org/10.1111/j.1365-3040.2004.01207.x

Burgess, S. S. O. & Downey, A. (2014). SFM1 Sap Flow Meter Manual. ICT International Pty Ltd.

Cáceres, L., Gomez-Silva, B., Monardes, V., Garró, X., Rodríguez, V., & Mckay, C. P. (2007). Relative humidity patterns and fog water precipitation in the Atacama Desert and biological implications. *Article in Journal of Geophysical Research Atmospheres*, *112*. https://doi.org/10.1029/2006JG000344

Cafferata, P., & Reid, L. (2013). Applications of long-term watershed research to forest management in California: 50 Years of Learning from the Caspar Creek Watershed Study. *California Forestry Report No. 5. Sacramento: State of California, The Natural Resources Agency, Department of Forestry & Fire Protection.* 110 p.

CAL FIRE. (2020). Historical Wildfire Activity Statistics. https://www.fire.ca.gov/stats-events/

Carbone, M. S., Still, C. J., Ambrose, A. R., Dawson, T. E., Williams, A. P., Boot, C. M., ... & Schimel, J. P. (2011). Seasonal and episodic moisture foresteds on plant and microbial contributions to soil respiration. *Oecologia*, *167*(1), 265-278.

Carbone, M. S., Park Williams, A., Ambrose, A. R., Boot, C. M., Bradley, E. S., Dawson, T. E., … Still, C. J. (2013). Cloud shading and fog drip influence the metabolism of a coastal pine ecosystem. *Global Change Biology*, *19*(2), 484–497. https://doi.org/10.1111/gcb.12054

Cárdenas, M. F., Tobón, C., & Buytaert, W. (2017). Contribution of occult precipitation to the water balance of páramo ecosystems in the Colombian Andes. *Hydrological Processes*, *31*(24), 4440–4449. https://doi.org/10.1002/hyp.11374

Corbin, J. D., Thomsen, M. A., Dawson, T. E., & D'Antonio, C. M. (2005). Summer water use by California coastal prairie grasses: fog, drought, and community composition. *Oecologia*, *145*(4), 511-521.

Dawson, T. E. (1998). Fog in the California redwood forest: ecosystem inputs and use by plants. *Oecologia*, *117*(4), 476-485.

Dawson, T. E., Burgess, S. S., Tu, K. P., Oliveira, R. S., Santiago, L. S., Fisher, J. B., ... & Ambrose, A. R. (2007). Nighttime transpiration in woody plants from contrasting ecosystems. *Tree Physiology*, *27*(4), 561-575.

Dymond, S. F., Richardson, P. W., Webb, L. A., Keppeler, E. T., Arismendi, I., Bladon, K. D., Cafferata, P. H., Dahlke, H. E., Longstreth, D. L., Brand, P. K., Ode, P. R., Surfleet, C. G., & Wagenbrenner, J. W. (In Review). A Field-Based Experiment on the Influence of Stand Density Reduction on Watershed Processes at the Caspar Creek Experimental Watersheds in Northern California. *Frontiers in Forests and Global Change.*

Dymond, S. F. (2016). *Caspar Creek Experimental Watersheds Experiment Three Study Plan: The influence of forest stand density reduction on watershed processes in the South Fork*. USDA Forest Service, Pacific Southwest Forest and Range Experiment Station, Davis, California. 28 p.

Earles, J. M., Sperling, O., Silva, L. C. R., Mcelrone, A. J., Brodersen, C. R., North, M. P., & Zwieniecki, M. A. (2015). Bark water uptake promotes localized hydraulic

recovery in coastal redwood crown. *Plant, Cell and Environment*. https://doi.org/10.1111/pce.12612

Eller, C. B., Lima, A. L., & Oliveira, R. S. (2013). Foliar uptake of fog water and transport belowground alleviates drought effects in the cloud forest tree species, D rimys brasiliensis (W interaceae). *New Phytologist*, *199*(1), 151-162.

Ewing, H. A., Weathers, K. C., Templer, P. H., Dawson, T. E., Firestone, M. K., Elliott, A. M., & Boukili, V. K. (2009). Fog water and ecosystem function: heterogeneity in a California redwood forest. *Ecosystems*, *12*(3), 417-433.

Fischer, D. T., Still, C. J., Ebert, C. M., Baguskas, S. A., & Park Williams, A. (2016). Fog drip maintains dry season ecological function in a California coastal pine forest. *Ecosphere*, *7*(6). https://doi.org/10.1002/ecs2.1364

Fischer, D. T., & Still, C. J. (2007). Evaluating patterns of fog water deposition and isotopic composition on the California Channel Islands. *Water Resources Research*, *43*(4), 1–13. https://doi.org/10.1029/2006WR005124

Fischer, D. T., Still, C. J., & Williams, A. P. (2009). Significance of summer fog and overcast for drought stress and ecological functioning of coastal California endemic plant species. *Journal of Biogeography*, *36*(4), 783–799. https://doi.org/10.1111/j.1365-2699.2008.02025.x

Fisher, J. B., Baldocchi, D. D., Misson, L., Dawson, T. E., & Goldstein, A. H. (2007). What the towers don't see at night: nocturnal sap flow in trees and shrubs at two AmeriFlux sites in California. *Tree Physiology*, *27*(4), 597-610.

Fuller, Wayne A. 1996. Introduction to Statistical Time Series. Chicago, Illinois: Wiley.

Griffith, R. S. (1992) Sequoia sempervirens. Fire Effects Information System [Online]. U.S. Department of Agriculture, Forest Service, Rocky Mountain Research Station, Fire Sciences Laboratory (Producer). Available: https://www.fs.fed.us/database/feis/plants/tree/seqsem/all.html.

Gultepe, I., Tardif, R., Michaelides, S. C., Cermak, J., Bott, A., Bendix, J., ... & Jacobs, W. (2007). Fog research: A review of past achievements and future perspectives. *Pure and applied geophysics*, *164*(6-7), 1121-1159.

Hammerschmidt, S. R., Dymond, S. F., Feng, X., Savage, J. A., & Wagenbrenner, J. W. (In Review). Understory Transpiration Rates Following Harvesting in a Coast Redwood Forest. *Ecohydrology*.

Harr, R. D. (1982). Fog drip in the Bull Run municipal watershed, Oregon. *Water Resources Bulletin*, *18*(5), 785-789.

Henry, N. (1998). Overview of the Caspar Creek Watershed Study. In: *Ziemer, R.R. (Ed.). Proceedings of the Conference on Coastal Watersheds: The Caspar Creek Story*. Gen. Tech. Rep. PSW GTR-168. Albany, California: U.S. Department of Agriculture, Service, Pacific Southwest Research Station; 149 p.

Hiatt, C., Fernandez, D., & Potter, C. (2012). Measurements of fog water deposition on the California Central Coast. *Atmospheric and Climate Sciences*, *2*(04), 525.

Hildebrandt, A., Al Aufi, M., Amerjeed, M., Shammas, M., & Eltahir, E. A. B. (2007). Ecohydrology of a seasonal cloud forest in Dhofar: 1. Field experiment. *Water Resources Research*, *43*(10). https://doi.org/10.1029/2006WR005261

Holder, C. D. (2003). Fog precipitation in the Sierra de las Minas Biosphere Reserve, Guatemala. *Hydrological Processes*, *17*(10), 2001–2010. https://doi.org/10.1002/hyp.1224

Houze, Robert A. Jr. – Cloud Dynamics (2014). Google Books. Retrieved January 10, 2020, from https://books.google.com/books?hl=en&lr=&id=GXEpAgAAQBAJ&oi=fnd&pg=PP1&dq=Houze,+R.+A.,+Jr.+(2014),+Cloud+Dynamics+International+Geophy&ots=jAgQZ1uF2X&sig=DkwO02xm1VK0tImhBnUc5-bDVtA#v=onepage&q=fog&f=false

Ingraham, N. L., & Matthews, R. A. (1988). Fog drip as a source of groundwater recharge in northern Kenya. *Water Resources Research*, *24*(8), 1406-1410.

Ingraham, N. L., & Matthews, R. A. (1995). The importance of fog-drip water to vegetation: Point Reyes Peninsula, California. *Journal of Hydrology*, *164*(1-4), 269-285.

Ingwersen, J. B. (1985). Fog drip, water yield, and timber harvesting in the Bull Run Municipal Watershed, Oregon. *JAWRA Journal of the American Water Resources Association*, *21*(3), 469-473.

Johnstone, J. A., & Dawson, T. E. (2010). Climatic context and ecological implications of summer fog decline in the coast redwood region. *Proceedings of the National Academy of Sciences*, *107*(10), 4533-4538.

Joslin, J. D., Mueller, S. F., & Wolfe, M. H. (1990). Tests of models of cloudwater deposition to forest canopies using artificial and living collectors. *Atmospheric Environment. Part A. General Topics*, *24*(12), 3007-3019.

Kendall, M. (1938). "A New Measure of Rank Correlation". *Biometrika*. **30** (1–2): 81–89. doi:10.1093/biomet/30.1-2.81. JSTOR 2332226.

Keppeler, E. (2007). Effects of timber harvest on fog drip and streamflow, Caspar Creek Experimental Watersheds, Mendocino County, California. In *In: Standiford, Richard B.; Giusti, Gregory A.; Valachovic, Yana; Zielinski, William J.; Furniss, Michael J., technical editors. 2007. Proceedings of the redwood region forest science symposium: What does the future hold? Gen. Tech. Rep. PSW-GTR-194. Albany, CA: Pacific Southwest Research Station, Forest Service, US Department of Agriculture; p. 85-94* (Vol. 194).

Kerfoot O. (1968). Mist precipitation on vegetation. *For. Abstr*., 29, 8–20.

Limm, E. B., Simonin, K. A., Bothman, A. G., & Dawson, T. E. (2009). Foliar water uptake: A common water acquisition strategy for plants of the redwood forest. *Oecologia*, *161*(3), 449–459. https://doi.org/10.1007/s00442-009-1400-3

Leipper, D. F. (1994). Fog on the U.S. West Coast: A Review. *Bulletin of the American Meteorological Society*, *75*(2), 229–240.

Mason Earles, J., Sperling, O., Silva, L. C., McElrone, A. J., Brodersen, C. R., North, M. P., & Zwieniecki, M. A. (2016). Bark water uptake promotes localized hydraulic recovery in coastal redwood crown. *Plant, cell & environment*, *39*(2), 320-328.

Means, Thos. H. (1927). Fog Precipitated by Trees. *Science*, *66*(1713), 402–403. Retrieved from https://about.jstor.org/terms

Mendiburu, Felipe de (2020). agricolae: Statistical Procedures for Agricultural Research. R package version 1.3-3. https://CRAN.R-project.org/package=agricolae

McJannet, D., Wallace, J. and Reddell, P. (2007), Precipitation interception in Australian tropical rainforests: II. Altitudinal gradients of cloud interception, stemflow, throughfall and interception. *Hydrol. Process.*, 21: 1703-1718. doi:10.1002/hyp.6346

Monteith, J. L. (1965). Evaporation and environment. In *Symposia of the society for experimental biology* (Vol. 19, pp. 205-234). Cambridge University Press (CUP) Cambridge.

National Cooperative Soil Survey. National Cooperative Soil Characterization Database. Available online. Accessed 3/27/2020.

Noss, R. F. (2000). *The redwood forest: history, ecology, and conservation of the coast redwoods*. Island Press, Covelo, USA

Oberlander, G. T. (1956). Summer fog precipitation on the San Francisco Peninsula. *Ecology*, *37*(4), 851–852. Retrieved from https://about.jstor.org/terms

Parsons, J. J. (1960). 'Fog drip' from coastal stratus, with special reference to California. *Weather*, *15*(2), 58–62. https://doi.org/10.1002/j.1477-8696.1960.tb00622.x

Pryet, A., Domínguez, C., Tomai, P. F., Chaumont, C., d'Ozouville, N., Villacís, M., & Violette, S. (2012). Quantification of cloud water interception along the windward slope of Santa Cruz Island, Galapagos (Ecuador). *Agricultural and Forest Meteorology*, *161*, 94–106. https://doi.org/10.1016/j.agrformet.2012.03.018

Olson, D. F., Roy, D. F., & Walters, G. A. (1990). Sequoia sempervirens (D. Don) Endl. Redwood. *Silvics of North America*, *1*, 541-551.

Pennsylvania State University. (2018). 10.2 - Autocorrelation and Time Series Methods | STAT 462. Applied Regression Analysis. https://online.stat.psu.edu/stat462/node/188/

R Development Core Team (2008). R: A language and environment for statistical computing. R Foundation for Statistical Computing, Vienna, Austria. ISBN 3-900051-07-0, URL http://www.R-project.org.

Rastogi, B., Williams, A. P., Fischer, D. T., Iacobellis, S. F., McEachern, K., Carvalho, L., … Still, C. J. (2016). Spatial and temporal patterns of cloud cover and fog inundation in coastal California: Ecological implications. *Earth Interactions*, *20*(15). https://doi.org/10.1175/EI-D-15-0033.1

Reid, L. M., & Lewis, J. (2009). Rates, timing, and mechanisms of rainfall interception loss in a coastal redwood forest. *Journal of Hydrology*, *375*(3–4), 459–470. https://doi.org/10.1016/j.jhydrol.2009.06.048

Ritter, A., Regalado, C. M., & Aschan, G. (2008). Fog water collection in a subtropical Elfin Laurel forest of the Garajonay National Park (Canary Islands): A combined approach using artificial fog catchers and a physically based impaction model. *Journal of Hydrometeorology*, *9*(5), 920–935. https://doi.org/10.1175/2008JHM992.1

Saksa, P., Safeeq, M., & Dymond, S. (2017). Recent patterns in climate, vegetation, and forest water use in California Montane Watersheds. *Forests*, *8*(8), 278. https://doi.org/10.3390/f8080278

Simonin, K. A., Santiago, L. S., & Dawson, T. E. (2009). Fog interception by Sequoia sempervirens (D. Don) crowns decouples physiology from soil water deficit. *Plant, Cell & Environment*, *32*(7), 882-892.

Schemenauer, R. S., Fuenzalida, H., & Cereceda, P. (1988). A neglected water resource: The Camanchaca of South America. *Bulletin of the American Meteorological Society*, *69*(2), 138-147.

Steinbuck, E. (2002). The influence of tree morphology on stemflow in a redwood region second-growth forest. *Master's Thesis, California State University, Chico. 55 p.*

Takahashi, K., Uemura, S., & Hara, T. (2011). A forest-structure-based analysis of rain flow into soil in a dense deciduous Betula ermanii forest with understory dwarf bamboo. *Landscape and ecological engineering*, *7*(1), 101-108.

Tolle, G., Polastre, J., Szewczyk, R., Culler, D., Turner, N., Tu, K., ... & Hong, W. (2005). A macroscope in the redwoods. In *Proceedings of the 3rd international conference on Embedded networked sensor systems* (pp. 51-63).

Torregrosa, A., Combs, C., & Peters, J. (2016). GOES-derived fog and low cloud indices for coastal north and central California ecological analyses. *Earth and Space Science*, *3*(2), 46–67. https://doi.org/10.1002/2015EA000119

Tukey, J. W. (1953). *The problem of multiple comparisons*. Unpublished paper, Princeton University, Princeton, NJ.

Underwood, S. J., Ellrod, G. P., & Kuhnert, A. L. (2004). A multiple-case analysis of nocturnal radiation-fog development in the central valley of California utilizing the GOES nighttime fog product. *Journal of Applied Meteorology*, *43*(2), 297-311.

U.S. EPA Office of Air Quality Planning and Standards (OAQPS). (2020). AirNow Air Quality Forecast. https://www.airnow.gov/?city=Fort%20Bragg&state=CA&country=USA

Westman, W. E., & Whittaker, R. H. (1975). The pygmy forest region of northern California: studies on biomass and primary productivity. *The Journal of Ecology*, 493-520.

Wickham, H. (2016). ggplot2: Elegant Graphics for Data Analysis. Springer-Verlag New York.

Williams, A. P., Still, C. J., Fischer, D. T., & Leavitt, S. W. (2008). The influence of summertime fog and overcast clouds on the growth of a coastal Californian pine: A tree-ring study. *Oecologia*, *156*(3), 601–611. https://doi.org/10.1007/s00442-008-1025-y

APPENDIX A: Field Methods

Ground Installation: Checklist and Methods Per Site

Soil Moisture Sensors (SoilVUE10)

- Locations
  - Near the bole of sapflux tree, halfway to canopy drip edge
  - At canopy drip edge
  - In nearby opening
- Data
  - Parameters collected:
    - Volumetric Water Content
  - Depths: 5, 10, 20, 30, 50, 100 cm
    - Collected at 15-min intervals
- Installation Checklist
  - 3 x SoilVUE10 sensors
  - 1 x 17-ft cable
  - 2 x 50-ft cable
  - Installation Kit (Figure 1) including:
    - A- auger extension shaft
    - B- hex socket
    - C- hex socket handle
    - D- Edelman auger
    - E- Auger clean-out tool
    - F- Rods for disassembly
    - G- T-handle for auger/extension shaft

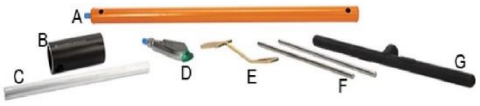

Figure 1: Installation

  - Sharpie
  - Field notebook
  - Spray bottle with water
  - Flagging
- Methods:
  - Use the tape/sharpie to mark the soil auger with the length of the SoilVUE10 sensor
  - Auger a vertical hole making sure not to go too deep or taper the sides of the hole (gaps will adversely affect measurements)
    - Set aside soil that was pulled from the top ~5cm to preserve the A/O horizon for later use
    - Make note of rocks you may hit or spot along the sides of the hole
  - Use spray bottle to wet the sensor and a few sprays into the hole (will lubricate and reduce the force necessary to install sensor)
  - Attach the hex socket to the top of the probe and begin screwing the probe into the hole (leave the plastic cap on the cable connector until the probe is completely installed)
  - When it is partially installed, remove ~5cm of soil from around the top of the hole (so the connector doesn't dig into the soil as the probe is being installed)
    - Keep this soil to pack in after sensor is fully installed
  - Stop when the top of the probe is flush with the soil surface

    - Align the cable connector to the soil moisture probe by aligning the keyed rings (**very easy to break, be extra careful**)
    - Tighten the cable connector so it is only finger tight
        - **do not overtighten, breaks easily**
    - Use the soil you removed from the top 5cm to carefully pack in around the sensor and cover with organic material
    - Flag location of the sensor, record distance and bearing from sapflux tree in field notebook
    - Route the cable to data logger
    - See Wiring Instructions for further steps

Campbell Scientific Leaf Wetness Sensor (LWS-33)

- Locations
    - 1 sensor installed ~2 ft. above ground
- Data
    - mV values collected at 15-min interval
- Installation Checklist
    - 4-ft mounting post
    - L-bracket
    - Nuts and bolts (in Ziploc bag labeled "LWS ground")
    - Zip ties
    - Measuring tape
    - Cloth and water for cleaning
    - Mallet / Fencepost pounder
    - Flagging
    - Sharpie
    - Field notebook
- Instructions:
    - Use sharpie to mark 2 ft (60 cm) on the mounting post that will be exposed above ground
    - Use the mallet to drive the post into the ground, stopping at the mark
    - Use the nuts and bolts from the Ziploc bag to secure the L-bracket to the top of the post
    - Using zip ties, secure the sensor to the L-bracket
        - Adjust the sensor so it is tilted ~15 degrees, do not overtighten
        - Tilting will allow water to run off instead of pooling on top of sensor
    - Ensure that the surface of the sensor is clean, pour some water and wipe off with a cloth
    - Secure cable to the post with zip ties and route to data logger
    - Flag the mounting bracket, record its distance and azimuth from the sapflux tree in field notebook
    - see Wiring Instructions for further steps
    -

Campbell Scientific CR1000 Data Logger and Enclosure

- Location

    - Best possible location determined by limiting cable lengths – will be determined
    - Mounted to (2) 6-ft tall struts
- Data
    - Collecting data from:
        - (3) SoilVUE10 Soil Moisture Sensors
        - (2) Leaf Wetness Sensors
        - (1) 03002 Wind Sentry: Wind Speed and Direction
        - (1) EE181 Temp/RH
- Installation Checklist
    - (1) Data Logger
    - (1) Enclosure
    - Mallet / fence-post driver
    - (1) 12-volt Battery
    - (1) Battery cable
    - (2) 6-ft long struts ("post")
    - Ziploc bag labeled "CDL" containing:
        - (4) Square washers
        - (4) Round washers
        - (4) 3" long 5/16 bolts
        - (4) Hex nuts
    - (1) Screwdriver for CR1000
    - Hex nut socket wrench/screwdriver
    - Pliers
    - Desiccants
    - Yale lock for CDL
    - Measuring Tape
- Instructions
    - Use mallet or fence post driver to drive one of the posts into the ground
    - Use measuring tape (or by holding up Enclosure, lining up the securing holes) to determine how far the other post needs to be positioned
    - Drive the other post into the ground, to a similar height
    - Secure with the washers, bolt and hex nuts, tightening with the socket wrench/screwdriver and pliers
    - Mount the data logger inside the enclosure
    - Wire battery and sensors to the logger
        - Battery Wiring:
            - Red - positive on battery / 12V on CR1000
            - Black – negative on battery / ground on CR1000
        - See Wiring Instructions for specifics
    - Connect to Field Laptop to verify sensors logging
    - When done, place desiccants and 12-volt battery inside the enclosure
    - Lock with Yale lock

Canopy Installation: Checklist and Methods

Canopy Mounting Frame (1 per plot)

- Location
  - Canopy of a safe-climbing tree
  - Inside or near the plot center
  - ~80 ft above ground
  - Facing NW direction (azimuth ~315°)
- Building Checklist
  - (4) 10-foot long 2x4 pieces
  - (4) 8-foot long 2x4 pieces
  - Miter saw
  - Impact driver
  - Box of 3" screws
  - 1-inch IPS, schedule 40 pipe: 1-ft long, unthreaded aluminum
  - (2) pipe clamps
  - Handsaw
  - Climbing gear and PPE
  - Extra rope for ascending the frame
  - (2) Ratchet straps
  - Torpedo level
  - 1 pack of shims

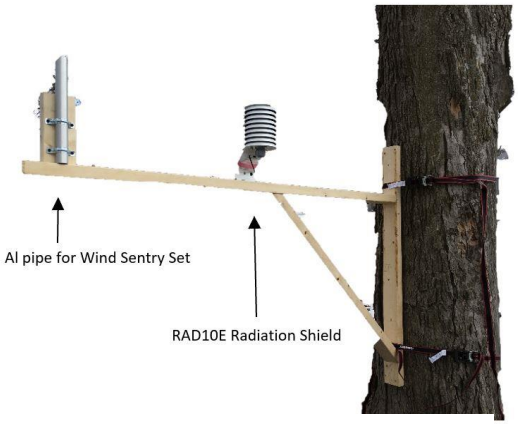

Figure 3: Canopy platform for mounting wind and temperature/RH sensors

- Instructions
  - Structure will be assembled in Fort Bragg prior to field day and will resemble Figure 3
  - Tie one end of the extra rope to the frame, leave it on the ground near the bole
  - Safely ascend the tree
  - Along the way, if necessary, clear a small path with the handsaw for pulling the mounting frame up
  - Isolate a location where the frame will be secured to the bole, clear away any obstructions
  - Attach the two sets of ratchet straps around the bole to have them in place
  - Assemble the extra climbing rope with a pulley and friction hitch
  - Pull the frame up, untangle and lead it between limbs if necessary
  - Once at the mounting location, slide the top of the frame under the top ratchet strap, tighten to secure it against the tree (refer to Fig. 3)
  - Slip the lower ratchet strap just above the support leg of the frame (as in Figure 3)
  - Use the torpedo level to make sure the horizontal arm of the frame is level with the ground
    - If not, place shims between the tree and vertical arm of structure until level
  - Tighten both straps to ensure their place

- Proceed with retrieving Wind Sentry Set and Radiation Shield to install on the mount

03002-130 Wind Sentry Set

- Location
  - Secured to aluminum pipe on the canopy mounting frame (Figure 3, Figure 4)
- Installation Checklist
  - 03002 Wind Sentry anemometer/ vane crossarm band clamp
  - Allen wrench provided with sensor
  - 5/64-inch Allen wrench
  - ½-inch open end wrench
  - Compass set to proper declination (see instructions below)
  - Zip ties
  - Small pair of pliers
  - (2) radio for communication between canopy/ground crews

- Instructions
  - Install the cup wheel to anemometer shaft using the Allen wrench provided with the sensor
  - Ascend the sensor into the canopy and place on top of the aluminum pipe
  - Orient the crossarm in the North/South direction with the vane to the north
    - Use a compass declination of 13° 56' East or +13.92 degrees
  - Ground crew:
    - Connect sensor to data logger (see Wiring Instructions)
    - Connect data logger to computer to watch real-time measurements
    - Note the wind direction measurement, communicate with canopy crew via radio
  - Canopy crew:
    - Rotate the sensor on the aluminum pipe until ground crew reports readings of 0 degrees
  - Once orientation is set to true north, tighten the mounting post band clamp
  - Route the sensor cable under the crossarm, securing to the mounting frame with zip ties
  - Route the cable down the bole of the tree and to the data logger

Campbell Scientific Leaf Wetness Sensor (LWS-66)

- Location
  - Attached to an L-bracket and installed 20 ft above ground
- Installation Checklist
  - (1) Leaf Wetness Sensor
  - Zip ties
  - L-bracket
  - (1) ratchet strap
  - Cloth and water for cleaning
- Instructions

- Use a ratchet strap to secure the L-bracket to the bole of a tree, facing an azimuth of ~315°
- Using zip ties, secure the sensor to end of the bracket so it is tilted ~15 degrees
- Ensure that the surface of the sensor is clean, pour some water and wipe off with a cloth
- Secure cable to the bracket using zip ties and route to data logger

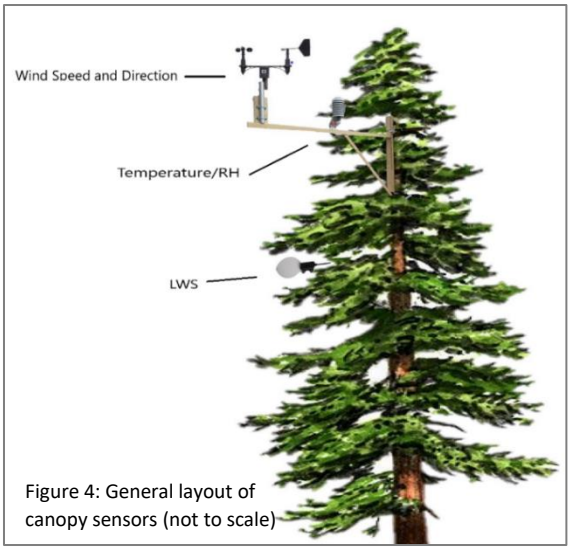

Figure 4: General layout of canopy sensors (not to scale)

EE181-130 Temperature/Relative Humidity

- Location
  - Housed inside the RAD10E and secured on the canopy mounting frame
- Checklist
  - (1) EE1181 Temperature/RH Sensor
  - (1) Cable, 130ft
  - (1) RAD10E Radiation Shield
- Instructions
  - Attach the cable to the sensor by aligning keyed connectors, pushing connectors together and finger tightening the knurled ring
    - Only finger tighten, using a wrench may damage the connector
  - Install the EE181 sensor in the RAD10E radiation shield:
    - The sensor gland nut on the bottom of the shield should be loose enough to insert sensor
      - If not, gently loosen it without breaking
    - Insert the EE181 sensor into the bottom of the shield
    - Situate the gland so it is 0.5-1” above the sensor connector (see Figure 5)
    - Tighten the nut around the gland until it firmly grips the body of the probe, use an adjustable wrench if necessary, but do not overtighten
  - Once canopy mounting frame is in place, cushion and raise the RAD10E containing the EE181 sensor into the canopy
  - Proceed with RAD10E mounting instructions

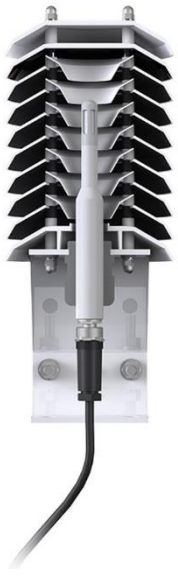
Figure 5: Placement of EE181 sensor within radiation shield

RAD10E 10-Plate Radiation Shield

- Location
  - Secured to canopy mounting frame (Figure 4)
  - Houses EE181 Temperature/Relative Humidity Sensor
- Installation Checklist
  - (2) 5/16” x 2.5” carriage bolts

    - (2) washers and nuts
- Instructions
    - Align the holes on the base of the RAD10E with the pre-drilled holes on the mounting frame
    - Secure to frame using nuts and bolts

APPENDIX B: Sensor and Program Information for CR1000

Table 1: **Sensors and their respective locations** that are routed to the CR1000 data logger. This table includes programming information such as thresholds, units and rates of measurement. Thresholds for the LWS measurements are in millivolts (mV).

Sensor Name	Note	Measuring Rate	Location at Site
SoilVUE10 (SM1)	SDI Address: 1	15 minutes	Between bole and canopy edge
SoilVUE10 (SM2)	SDI Address: 2	15 minutes	Canopy edge
SoilVUE10 (SM3)	SDI Address: 3	15 minutes	Opening
LWS	Dry Threshold: <274 Wet Threshold: >/= 284	60 seconds	Mounted 2 ft above ground
LWS Canopy	Dry Threshold: <274 Wet Threshold: >/= 284	60 seconds	Canopy
03002 Wind Speed and Direction	Wind Speed: m/s Wind Direction: degrees	60 seconds	Canopy
EE181 Temperature/RH	Air Temp: °C Relative Humidity: %	60 seconds	Canopy

Table 2: **Fifteen-minute output table** generated by the CR1000 with a specified unit of measurement, output type and notes for a given sensor. VWC refers to volumetric water content and mV is millivolts.

Sensor Name	Measurement	Output	Note
SoilVUE10 (SM1)	VWC	Average	Depth (cm): 5, 10, 20, 30, 50, 100
SoilVUE10 (SM2)	VWC	Average	Depth (cm): 5, 10, 20, 30, 50, 100
SoilVUE10 (SM3)	VWC	Average	Depth (cm): 5, 10, 20, 30, 50, 100
LWS	mV	Average	
LWS Canopy	mV	Average	

Table 3: **Hourly (60-minute) output table** generated by the CR1000 with specified units of measurement, output type and notes for a given sensor.

Sensor ID	Measurement	Output	Note
SoilVUE10 (SM1)	VWC	Average	Depth: 5, 10, 20, 30, 50, 100
SoilVUE10 (SM2)	VWC	Average	Depth: 5, 10, 20, 30, 50, 100
SoilVUE10 (SM3)	VWC	Average	Depth: 5, 10, 20, 30, 50, 100
LWS	mV	Average	
LWS Canopy	mV	Average	
03002 Wind Speed	m/s	Average	
		Maximum	Recording time of maximum
03002 Wind Direction	degrees	Wind Vector	Considers mean horizontal speed and mean direction of unit vector
EE181 Air Temperature	°C	Average	
EE181 Relative Humidity	Percent	Minimum	
		Maximum	Recording time of maximum

APPENDIX C: Supplemental Tables

Table C1: Results of Welch's two sample t-test comparing mean daily fog deposition between sites ($\alpha = 0.05$). The H_0 states that the means of each site combination are not significantly different from one another at the $\alpha = 0.05$ level. Effective degrees of freedom (df) are adjusted for autocorrelation and unequal variance between sites.

Sites Compared	**t- statistic**	**Effective df**	**p-value**
Forested shoulder, Forested ridge	5.438	150.21	<0.01
Forested shoulder - Harvested shoulder	-0.085	213.36	0.93
Forested shoulder - Harvested ridge	5.694	127.52	<0.01
Forested ridge - Harvested shoulder	-7.236	176.96	<0.01
Forested ridge - Harvested ridge	0.0053	183.32	0.99
Harvested shoulder - Harvested ridge	7.847	136.91	<0.01

Table C2: Results of Welch's two-sample, two-tailed t-test comparing the mean GWC (%) of litter among sites using $\alpha = 0.05$ and adjusted sample size.

Sites Compared	t- statistic	Effective df	p-value
Forested shoulder, Forested ridge	0.363	11.67	0.723
Forested shoulder - Harvested shoulder	2.858	9.03	0.019
Forested shoulder - Harvested ridge	2.381	10.77	0.037
Forested ridge - Harvested shoulder	5.851	4.82	0.002
Forested ridge - Harvested ridge	4.326	7.52	0.003